Particle Number Size Distribution of Wintertime Alpine Aerosols and Their Activation as Cloud Condensation Nuclei in the Guanzhong Plain, Northwest China

Yukun Chen[1,2], Xin Wang[2,1†], Wenting Dai[2], Qiyuan Wang[2], Xiao Guo[2], Yali Liu[3], Weining Qi[2], Minxia Shen[2], Yifan Zhang[3], Lu Li[2], Yue Cao[3], Yueshe Wang[1*], Jianjun Li[2,4*]

[1] State Key Laboratory of Multiphase Flow in Power Engineering, Xi'an Jiaotong University, Xi'an 710049, China;
[2] State Key Laboratory of Loess and Quaternary Geology, Key Lab of Aerosol Chemistry and Physics, Institute of Earth Environment, Chinese Academy of Sciences, Xi'an 710061, China
[3] Xi'an Institute for Innovative Earth Environment Research, Xi'an 710061, China
[4] National Observation and Research Station of Regional Ecological Environment Change and Comprehensive Management in the Guanzhong Plain, Shaanxi, China

*Corresponding authors:
Prof. Yueshe Wang (wangys@mail.xjtu.edu.cn)
State Key Laboratory of Multiphase Flow in Power Engineering, Xi'an Jiaotong University, Xi'an, China;
Phone: +86-29-82667323
Orcid ID:0000-0003-1767-3175

Prof. Jianjun Li (lijj@ieecas.cn)
Institute of Earth Environment, Chinese Academy of Sciences, Xi'an 710061, China
Phone: 86-29-6233-6273
Fax: 86-29-6233-6234
Orcid ID:0000-0002-3485-5379

†Co-first author:
This author contributed equally to this work and should be considered co-first author.

Key points:

- Small diameter particle increased from NPF erupted frequently in 13:00-18:00 and had a potential contribution to CCN in the growth process.
- More hygroscopic and larger particles were small index k, while the hydrophobic and small particles were opposite in winter observation.
- The hygroscopicity parameter decreased from 0.22 to 0.13 with the supersaturation from 0.2 to 1.0% in the Alpine region.

Abstract:

In this study, particle number size distribution (PNSD) and concentration of cloud condensation nuclei (N_{CCN}) were observed at the summit of Mt. Hua during Dec. 16th 2020 - Jan. 23rd 2021. The concentration of nucleation mode particles with the growth ratio of 0.83 nm·h^{-1} erupted frequently from 13:00 to 18:00 local time due to the intense photochemistry. The explosive increase of the small diameter particles could not be activated into droplets, but they had the potential to adsorb or absorb the polluted gaseous to promote the growth conversion into CCN. In the growth process, relative humidity had reverse effect on diameter and concentration with temperature, while higher wind speed was beneficial for the removal of large particles. SO_2 and NH_3 had a synergistic effect in contributing to the increase of particle diameter and concentration for the relative larger diameter, but NH_3 had inverse effect on the number concentration for the nucleation mode particles. Additionally, the influence of O_3 on the distribution characteristics of particle may be regulated by temperature. The small k value that fitted by two-parameter power model suggested the larger or hygroscopic particles, while larger value for the ultrafine or hydrophobic particles. Hygroscopicity parameters (κ) showed a downward trend with the increase of supersaturation as the source direction of the air mass gradually shifted from northwest to southwest. By comparing the calculated and the measured N_{CCN}, we inferred that the hygroscopicity parameter decreased from 0.22 to 0.13 with the supersaturation from 0.2 to 1.0% in Alpine region.

Plain Language Summary:

This manuscript reported the characteristics of particle number size distribution of alpine aerosols and their activation as cloud condensation nuclei on Mt. Hua in winter, 2020. We found that the number concentration of nucleation mode particles with the growth ratio of 0.83 nm·h^{-1} erupted frequently from 13:00 to 18:00 local time due to the intense photochemistry. In addition, the small diameter particle increased from NPF and had a potential contribution to CCN through the process of the growth, which was affected by air masses, meteorological conditions, and gaseous pollutants. Subsequently, we fitted the correlation between N_{CCN} and supersaturations, and found that the small k value that fitted by two-parameter power model suggested the larger or hygroscopic particles, while larger value for the ultrafine or hydrophobic particles. Finally, we calculated the hygroscopicity parameters (κ) that showed a downward trend with the increase of supersaturation due to the shift of the air masses. By comparing the calculated and measured N_{CCN}, we inferred that the hygroscopicity parameter decreases from 0.22 to 0.13 with the supersaturation from 0.2 to 1.0% in the Alpine region.

1 Introduction

Aerosols suspended in the atmosphere can influence the climate by direct and indirect effects (Kim et al., 2017). Direct effects include the aerosol particle interactions with radiative forcing by scattering, absorption, and reflection, resulting in warming or cooling of the atmosphere (Konovalov et al.; Ramana et al., 2007; Ramanathan et al., 2007; Saturno et al., 2018; Seinfeld et al., 2016). Indirect effects include aerosol particle acting as cloud condensation nuclei (CCN) or ice nuclei (IN), thereby affecting the microphysical and macrophysical properties of different types of clouds, radiation, dynamics, precipitation, and lifetime (Chang et al., 2017; Charnawskas et al., 2017; Peng et al., 2020; Poschl and Shiraiwa, 2015; Sebastian et al., 2021; Seinfeld et al., 2016; Wang et al., 2018b; Zhang et al., 2015). Nevertheless, the role of aerosols in the environment often tends to be estimated with large uncertainty due to much is known on the indirect effects of aerosols (Hung et al., 2014; Ramanathan et al., 2005; Seinfeld et al., 2016; Xu et al., 2021a).

Aerosols can be divided into four modes according to the aerosol particle diameter, that is, the nucleation mode (<~30nm), Aitken mode (~30-100nm), accumulation mode (100-1000nm), and coarse mode (>1000nm). The ambient aerosol particle number size distribution (PNSD) associated with direct particle emissions, in situ formation processes, atmospheric interactions between particles or between particles and gaseous compounds, and deposition processes (Wu and Boor, 2021). Furthermore, aerosol properties exhibit significant difference in the atmosphere largely depending on interaction between local and regional sources and atmospheric processing (Monteiro dos Santos et al., 2021). Almost all particles in the range of nucleation mode are new particles formed by gaseous precursors (Franco et al., 2022; Sebastian et al., 2021; Wu and Boor, 2021). Wang et al. (2014) discussed the variations in the aerosol number spectrum and the NPF events for various types of air masses in combination with meteorological data (Wang et al., 2014). Subsequently, the fresh formed clusters adsorb more gaseous molecules increasing their diameter, and gradually transit to nucleation mode and Aitken mode. Li et al. (2011) identified the individual aerosol particles with

105 TEM, monitored the NPF and growth events by a wide-range particle spectrometer, and
106 analyzed ion concentrations in $PM_{2.5}$(Li et al., 2011b). When in high supersaturation
107 conditions or cloud processes, the growing particles acting as cloud condensation nuclei
108 can be activated to become cloud droplets.

109 Some researchers found that the number of aerosols from new particle formation
110 (NPF) can contribute about half of the global CCN (Andreae et al., 2022; Cai et al.,
111 2021; Franco et al., 2022; Zhao et al., 2021). Particles are activated under the
112 supersaturation (SS) environment when the particle size is larger than the critical
113 particle size related to the hygroscopicity parameter, κ. According to the Köhler theory,
114 the larger the particle is, the easier it is to be activated. That is, the relationship between
115 κ value and critical particle size is inversely proportional (Petters and Kreidenweis,
116 2007). Thus, aerosol particles in the Aitken mode and accumulation mode are apt to act
117 as cloud condensation nuclei to be activated into cloud droplets, which affects the
118 microphysical process of cloud. Although nucleation mode aerosol particles, which
119 require relative higher supersaturation to be activated, are derived from the event of
120 NPF, the subsequent growth of new aerosol particles can still affect cloud condensation
121 nuclei under low relative humidity (Fan et al., 2018; Kulmala and Kerminen, 2008;
122 Ueda et al., 2016). The CCN number concentration (N_{CCN}) is crucial in characterizing
123 aerosol–cloud interaction and their radiative impacts. So far, observation and analysis
124 of aerosols and CCN were mainly focused on the sites of urban, rural, forested, coastal
125 and remote mainland areas (Wang et al., 2014). However, such study on Alpine region
126 of aerosol is still limited. The technologies that have been used to study the Alpine
127 region of aerosols and CCN include UAV aviation flight (Li et al., 2019; Manoj et al.,
128 2021), remote sensing technology and in-situ measurement(Li et al., 2020; Li et al.,
129 2014). Observation on the top of mountain sites make it possible to investigate regional
130 aerosol and CCN in the free troposphere, and its interactions with free troposphere-
131 boundary layer (Varghese et al., 2016). Some ground sites observation had been carried
132 out to monitor the N_{CCN} as well as the hygroscopicity, but their result cannot
133 straightforward be extrapolated to the vicinity or the bulk of the cloud due to the vertical
134 distribution differences. In addition, observation of N_{CCN} at Alpine sites can directly

reflect the characteristics of the particles that become cloud condensation nuclei. Li et al. (2017) investigated the chemical composition of cloud samples and droplet size distributions at the summit of Mt. Tai (Li et al., 2017a). The variations in the CCN properties are strongly influenced by the number size distribution, chemical composition and mixing state of aerosols (Eleftheriadis et al., 2020; Manoj et al., 2021; Vu et al., 2019). Although it is also one of the key factors affecting aerosol activation to become cloud condensation nuclei, the particle mixing state will cause differences in N_{CCN} prediction due to the changes in component (Gaston et al., 2018; Hughes et al., 2018; Ma et al., 2017; Stevens and Dastoor, 2019; Vu et al., 2019; Xu et al., 2021b; Zhang et al., 2022). Vu et al. suggested that the internal and external mixing of succinic acid and sodium chloride did not affect the change of CCN number concentration, while the number of activated CCN changed greatly with the variation of particle size and mixing ratio after the combustion aerosol was mixed with NaCl and $(NH_4)_2SO_4$ (Vu et al., 2019). However, other researchers investigated the mixing state of aerosols by monitoring the hygroscopic GF-PDF distribution of environmental aerosols and black carbon (Li et al., 2018; Stevens and Dastoor, 2019; Wang et al., 2018a; Xu et al., 2021b; Zhang et al., 2022). On the contrary, Kammermann et al. showed that the particle mixing state has little effect on N_{CCN} prediction in the polar regions with few influence from anthropogenic sources (Kammermann et al., 2010). In addition, some researchers are engaged in this research, that is, using real-time aerosol chemical composition measurement to estimate N_{CCN} (Arub et al., 2020; Cai et al., 2018; Kim et al., 2017; Mallet et al., 2016; Patel and Jiang, 2021). However, the accurate hygroscopicity parameter of organic matter has become an obstacle to the estimation of N_{CCN}. In generally, when the chemical composition is unknown, the κ value of hygroscopicity parameters can be assumed to calculate the activation critical particle size according to Köhler theory, and then the activated N_{CCN} can be calculated in combination with PNSD spectrum (Jayachandran et al., 2017; Kammermann et al., 2010; Rejano et al., 2021; Wu et al., 2017; Xu et al., 2021a). The calculation process of general N_{CCN} is summarized by Kammermann et al. and Xu et al. (Kammermann et al., 2010; Xu et al., 2021a). Therefore, the hygroscopicity of aerosol particles forming cloud condensation

nuclei can be directly obtained by measuring them on high mountains with SMPS-CCN instruments that is a comparison between the measured and the extrapolated N_{CCN} (Xu et al., 2021a).

In this study, measurements on time-resolved PNSD of aerosol and N_{CCN} were carried out for the first time at the summit of the West Peak of Mt. Hua. The measurements were from Dec. 16th 2020 to Jan. 23rd as a winter campaign to explore the basic characteristics of particulate matter. Simultaneously, the formation and dissipation of clouds for Alpine areas can be figured out by the aerosols from external long-distance transportation, anthropogenic emissions and natural source emissions with the method of revealing the characteristics of Alpine aerosol particles and the mechanism of CCN formation. Thus, aerosols and CCN could be observed directly and effectively on the West peak of Mt. Hua since the sampling site was closed to the margin or in the bulk of the cloud. The results of observation would reveal the interaction between aerosols and clouds and the potential for aerosols to form clouds in northwest China. In this paper, the structure of the paper was as follows. Firstly, the sampling location, instrument method and data calculation process were introduced. In addition, we analyzed the diurnal variation of aerosol PNSD for five divided episodes and its correlation with meteorological parameters and gaseous pollutant. What' more, the diurnal variation characteristics of N_{CCN} with supersaturation were also analyzed and fitted with a C and k two-parameter power model. Finally, the critical truncation diameter and hygroscopicity parameter were calculated, and the calculated N_{CCN} was compared to the actual measured N_{CCN}.

2. Method

2.1 Sampling site

The meteorological station is located at the summit of the West Peak of Mt. Hua (34.48'N, 110.08' E, 2060 m a.s.l, Figure 1 and S1), which is about 130 km away from the east of the Xi'an City. Although this summit sampling site, as description in the paper published by Li et al. (Li et al., 2011a; Li et al., 2013), is a tourist attraction, our sampling was conducted during the annual overhaul and maintenance of the uphill

cableway for tourists and hence the influence of summit anthropogenic sources was negligible. Meteorological parameters on the summit of the West Peak including temperature, relative humidity (RH), pressure, visibility, wind speed, wind direction, and precipitation were monitored and recorded over the measurement campaign. In addition, the data of the boundary layer height and surface net solar radiation during the sampling period were downloaded from the Climate Data Store website (https://climate.copernicus.eu/climate-data-store). Before the sampling, the time of all instruments was adjusted to the local zone time, and the recorded data were also corresponding to the local zone time.

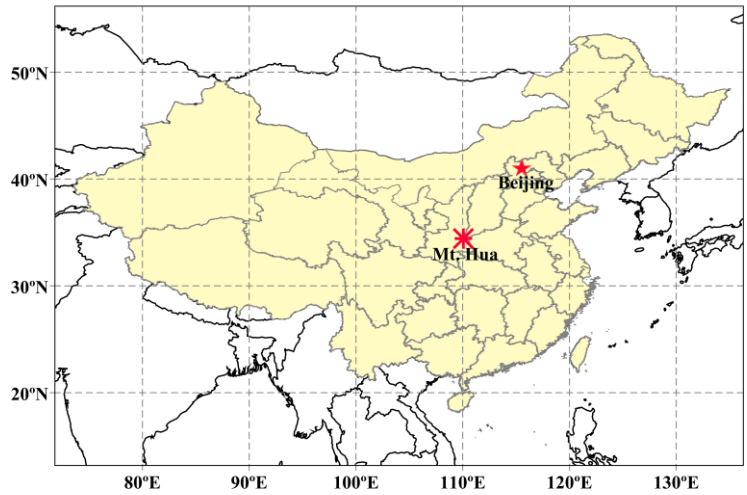

Figure 1. Location of the sampling site at Mt. Hua in central China (image from © Meteoinfo Software)

2.2 Gaseous pollutants

Two trace gas analyzers, Thermo 48i and Thermo 43i (Thermo Fisher Scientific Inc., Waltham, MA, USA), were used to monitor the concentration of CO and SO_2, respectively (Monteiro dos Santos et al., 2021; Wang et al., 2019). O_3 concentration was monitored using an ultraviolet photometer based on the ultraviolet absorption spectrometry (EC9810B, ECOTECH, Australia) (Hakim et al., 2019). NH_3 concentration was monitored in real time by a high-precision cavity ringdown spectrometer (CRDS) (G2103, Piccaro, USA), and a detailed description is provided in supplementary materials (Text S1). (He et al., 2020; Martin et al., 2016; Wentworth et al., 2016). NO_x concentration was also monitored but its concentration is lower than the detection limit of the Thermo 42i-D analyzer (Thermo Fisher Scientific Inc., Waltham,

MA, USA) and therefore the data is not discussed in this work.

2.3 Particle number-size distribution (PNSD) of aerosol

Scanning Mobility Particle Sizer Spectrometer (SMPS) was employed to monitor particle number-size distribution of aerosol (PNSD). The SMPS is composed of an electrostatic classifier (3082, TSI Inc., USA), a Nano Differential Mobility Analyzer (Nano-DMA, 3085, TSI Inc., USA) or a Long Differential Mobility Analyzer (Long-DMA, 3081, TSI Inc., USA), a N-butanol based Condensation Particle Counters (CPC, 3775, TSI Inc., USA). The SMPS was placed in an air-conditioned room of 25℃ and a pierce of sampling tube (1/4 inches) made of conductive silicone was stretched out of the window for a certain distance. In order to ensure the accuracy and reliability of data, the flow rates were adjusted every 3 days, 203 nm Polystyrene Latex (PSL) calibration and in-situ intercomparison (ACTRIS Round Robin Tour) according to the ACTRIS and GAW recommendations (Rejano et al., 2021; Stolzenburg et al., 2018; Wiedensohler et al., 2012) was performed at the beginning of the campaign, and multiple charge correction and diffusion loss corrections were applied to all data (Dameto de España et al., 2017). In general, the ratio of aerosol and sheath flowrates was set to 1:10 (0.3 and 3 $L \cdot min^{-1}$, respectively), and data acquisition was recorded every 5 min.

In order to obtain extensive information of particle distribution on Mt. Hua, two-phase sampling campaigns were designated. The first-phase one was from Dec. 16th to 24th, 2020 (denoted as T1) when a Nano-DMA was employed in monitoring the aerosol particles with a size ranging from 4.45 to 162.5nm with particular interest in nucleation mode of particulate matter (Eleftheriadis et al., 2020; Li et al., 2019; Pryor et al., 2016; Stolzenburg et al., 2018; Wang et al., 2020; Weller et al., 2015). The second-phase one was from Jan. 9th to 23th, 2021 (denoted as T2) when a Long-DMA replacing Nano-DMA was adopted for scanning number-size distribution of Atiken and accumulation mode particles with a size ranging from 14.1 to 736.5nm. (Baalbaki et al., 2021; Han et al., 2013; Monteiro dos Santos et al., 2021; Zhang et al., 2018).

2.4 Cloud droplet nucleation measurements

A continuous-flow streamwise thermal-gradient single column Cloud Condensation Nuclei counter (CCN-100, Droplet Measurement Technologies, USA) was employed for measuring N_{CCN} at a time resolution of 1 Hz for five supersaturation (SS) values (SS=0.2%, 0.4%, 0.6%, 0.8%, 1.0%) during the period from Dec.16th, 2020 to Jan. 23rd, 2021. The CCN counter was installed in parallel with the SMPS by a Y-type tee joint connected to the outlet of the self-made silica gel diffusion dryer. During sampling, an amount of 0.5 lpm of ambient air dividing into aerosols and sheath stream at the ratio of flowrate of 1:10 was flowing into the chamber of the CCN counter (Rejano et al., 2021). A constant water vapor supersaturation would be established along the centerline of the column because water molecules from column wall diffused more quickly than heat transfer. Once the aerosol particles were continuously exposed to the varying SS conditions generated inside the column, some of them whose critical supersaturation less than the given supersaturation would act as CCN to be activated into droplets (Jayachandran et al., 2018). In general, the diameter of activated particles is considered to lies in the range of 0.75-10 μm, and the sampling time for each SS was set in such a way that the total cycle period of five supersaturations was completed in 30 min with 0.20% SS for 10 min and 5 min each for other SS (Singla et al., 2017).

Prior to sampling, the CCN counter was calibrated by operating in parallel with a CPC downstream of the DMA that classified monodispersed $(NH_4)_2SO_4$ aerosols originated from drying of aqueous droplets generated by atomizer (Rose et al., 2008; Rose et al., 2010). For the sake of data reduction, we follow the ACTRIS standardized protocol (available in http://actris.nilu.no/Content/SOP) for N_{CCN} data. According to this protocol, the raw data of CCN have been filtered as follows: firstly, only data with SS above the 1st percentile and below the 99th percentile have been taken into account for each SS setpoint value. Then for each SS value, we computed the average value and the standard deviation (STD). Secondly, data above and below 1.5 times the STD were flagged as invalid and not further used. Normally the first and last points in each SS step were the points that did not satisfy the criteria because the SS conditions in the growth chamber are not yet stable (Rejano et al., 2021).

2.5 Parameters derived from the SMPS and CCN spectra

The applicability of lognormal particle size distributions in describing the properties of aerosol size distributions have been discussed in several papers (Koponen, 2003; Monteiro dos Santos et al., 2021; Ueda et al., 2016; Yu et al., 2019; Zhao et al., 2021). All the particle number size distributions could be fitted using unimodal or bimodal lognormal modes: nucleation modes (<30 nm), Aitken mode (30–100 nm), and up to an accumulation mode (>100 nm) (Monteiro dos Santos et al., 2021). The geometric mean diameter (GMD) and the geometric standard deviation (σ) is often quoted and specify the distribution (Grainger, 2020):

$$\mathrm{GMD} = \exp\left(\frac{\sum_i N_i \ln(D_i)}{\sum_i N_i}\right) \tag{1}$$

$$\sigma = \exp\left\{\left[\frac{\sum N_i \left(\ln d_i - \ln(\mathrm{GMD})\right)^2}{N-1}\right]^{\frac{1}{2}}\right\} \tag{2}$$

where N_i is for the particle number in each corresponding bin, D_i stands for the diameter of in each bin, N is for the total particle number of aerosols.

The calculation of particle growth and formation rates along with the condensation sink was done according to the procedure described by Kulmala et al. (2012) (Baalbaki et al., 2021; Kulmala et al., 2012; Kulmala et al., 2004; Qi et al., 2015). The growth rate (GR) of particles, a central parameter for quantifying the diameter of particles reaching climatically relevant sizes, can be expressed as:

$$\mathrm{GR} = \frac{\mathrm{d}d\mathrm{p}}{\mathrm{d}t} = \frac{\Delta d\mathrm{p}}{\Delta t} = \frac{d_{\mathrm{p}_2} - d_{\mathrm{p}_1}}{t_2 - t_1} \tag{3}$$

where d_{p1} and d_{p2} are the mean values of the size bin of nucleation mode particles corresponding to the maximal number concentration at the times t_1 and t_2, respectively.

The key parameterization of CCN spectra, which is the curve that relates N_{CCN} to SS, is the power law derived by Twomey (1959) (Jayachandran et al., 2017; 2018; Rejano et al., 2021; Twomey, 1959; Varghese et al., 2016):

$$N_{\mathrm{CCN}}(SS) = C \bullet SS^k \tag{4}$$

where C and k are empirical fit parameters. The C parameter represents the N_{CCN} at

corresponding SS and tracks aerosol concentration variation. The higher the C value is, the higher the aerosol particles load is (Rejano et al., 2021; Shen et al., 2019). The parameter of k is a dimensionless exponent and gives information about the steepness of the CCN spectra. Therefore, an aerosol population dominated by hygroscopic or big aerosol particles would have flat CCN spectra and low values of k, while steep CCN spectra and high k values are related to hydrophobic or ultrafine particles, which would need higher SS to be activated into droplets (Rejano et al., 2021).

Activation ratio (AR) is the fractional contribution of N_{CCN} to total aerosol number concentration (N_{CN}), which is one of the most crucial information required for understanding the aerosol-cloud interactions and its radiative forcing (Burkart et al., 2011; Chen et al., 2019; Dusek et al., 2003; Hung et al., 2014; Jayachandran et al., 2017; 2018; Kim et al., 2018). The N_{CCN} calculated from the particle number size distributions (N_{CCN}(PNSD)) is obtained by integrating the PNSD of particles larger than the critical dry particle diameter (D_{crit}) (Shen et al., 2019; Wu et al., 2017; Xu et al., 2021a),

$$N_{CCN}\left(\mathrm{PNSD}\right)=\int_{D_{crit}}^{D_{upper}} n_{CN}\left(\log D_p\right) d\left(\log D_p\right) \tag{5}$$

where, the D_{upper} represents for the upper limitation of PNSD, which is D_{upper}=736.5nm, in this study. D_{crit} is the activated diameter particles. If D_{crit} is equal to the lower limitation of the particle number-size spectrum, i.e. D_{crit}=D_{lower}=14.1nm in this study, then all the particles are activated with the AR=1. n_{CN}(logD_p), aerosol particle number size distribution, is equal to the dN/dlogD_p (Mallet et al., 2016).

In general, the value of D_{crit} depend on the SS, which can be related to the single parameter hygroscopicity, κ, to describe the CCN activity and to determine the effect of mixing states of multiple components on the supersaturated hygroscopic properties of aerosols (Petters and Kreidenweis, 2007; Vu et al., 2019). Thus, the hygroscopicity parameters, κ, corresponding to the activated diameter values can be calculated by Eq.(6) and Eq.(7) (Dusek et al., 2010; Kammermann et al., 2010; Kim et al., 2018; Miao et al., 2015; Wu et al., 2017; Xu et al., 2021a):

$$\kappa=\frac{4A^3}{27D_{crit}^3\ln^2 SS} \tag{6}$$

$$A = \frac{4\sigma_{s/a} M_w}{RT\rho_w} \quad (7)$$

where T is the absolute temperature (298.15 K), R is the universal gas constant (8.314 $J \cdot K^{-1} \cdot mol^{-1}$), ρ_w is the density of water (997.1 $kg \cdot m^{-3}$), M_w is the molar mass of water (0.018 $kg \cdot mol^{-1}$), and $\sigma_{s/a}$ is surface tension at the droplet–air interface (assumed to be 0.072$N \cdot m^{-1}$).

3 Results and discussion

3.1 Characteristic of PNSD

3.1.1 Nucleation mode

Previous field observations frequently recorded that the upper size of nucleation mode particles was in the range of 20-30nm (Chen et al., 2017; Gogoi et al., 2014; Kompalli et al., 2014; Willis et al., 2016; Zhang et al., 2017) (see a summary in Table S1). According to the PNSD (shown in Figure S2) in 4.45 - 162.5 nm during Dec. 16th - 24th, 2020, particles with higher number concentration were mainly distributed in the range of nucleation and accumulation modes. However, the measurement of particles in accumulation modes was incomplete due to the limitation of SMPS, which was not discussed in detail in this study. Therefore, the variation characteristics of aerosols in nucleation mode with a diameter less than 30 nm were emphasized in detail in this study. Figure S2 shows that the number concentration of particles increased sharply in the range of 10-30nm during the period of 13:00-18:00 pm, and the unimodal distribution pattern of nucleation mode shift to larger diameter range due to particle growth, resulting in the increase of average geometric particle size with time (Wang et al., 2014). Figure 2 presents the variation of average diurnal PNSD in the sampling period from Dec. 16th to 24th, 2020, for particle diameter smaller than 30nm. The numbers of particles were relatively stable corresponding to their $dN/d(\log D_p)$ much lower than 2000#$\cdot cm^{-3}$ from 0:00 to 12:00, and particles with a diameter less than 8nm were almost lower than 400#$\cdot cm^{-3}$ down to zero (Figure 2a). This result meant that there was a little ultrafine new particulate matter existing as the background in alpine aerosols on Mt. Hua in winter. Nevertheless, the number of particles with a diameter from 10nm to 20nm increased sharply from 14:00 to 17:00pm with the $dN/d(\log D_p)$ between 2000 and 4000#$\cdot cm^{-3}$, accompanied by the broadening of the lognormal distribution of

particles in nucleation mode, which meant the increase of particle size. Subsequently, the number concentration of particles began to decline after 17:00pm with the narrowing of unimodal lognormal distribution. Furthermore, the particle size corresponding to the maximum concentration increased briefly from 13:00 to mid-night. Therefore, the particle GR can be fitted linearly with time from diurnal average data of particulate matter sampled on Mt. Hua according to Eq. (3). In this study, the fitted GR was 0.83 $nm \cdot h^{-1}$, which was apparently lower than one on the ground areas and other mountain sites (Babu et al., 2016; Deng et al., 2020; Gao et al., 2011; Gao et al., 2009; Kanawade et al., 2014; Lampilahti et al., 2021; Liu et al., 2008; Minoura and Takekawa, 2005; Mönkkönen et al., 2005; Sebastian et al., 2021; Yue et al., 2009) (Table S2). Generally, particle GRs in urban locations tend to be higher than those in rural or remote environments, but are still of the same order of magnitude of 1-10 $nm \cdot h^{-1}$ (Kerminen et al., 2018; Yu et al., 2017). Thus, it can be inferred from the slow growth of aerosol particle diameter that the condensation or reaction rate of pollutants on the particle surface is low on the alpine region, which is not beneficial for the growth of particles. The profiles of diurnal mean variation of particles concentration and GMD with diameter smaller than 30nm, $GDM_{<30}$, were plotted in Figure 2(b). We observed GMD reached the lowest value at 14:00 pm that was consistent with the time when the surface net solar radiation reached the maximum value (Figure S4), accompanied by the highest degree of photochemical reaction. Thus, the sharp burst of particle number concentration in nucleation mode originate from new particle formation (NPF) might be caused by the intense photochemical reaction. The GMD of particles decreased rapidly due to the thousands of ultrafine particles.

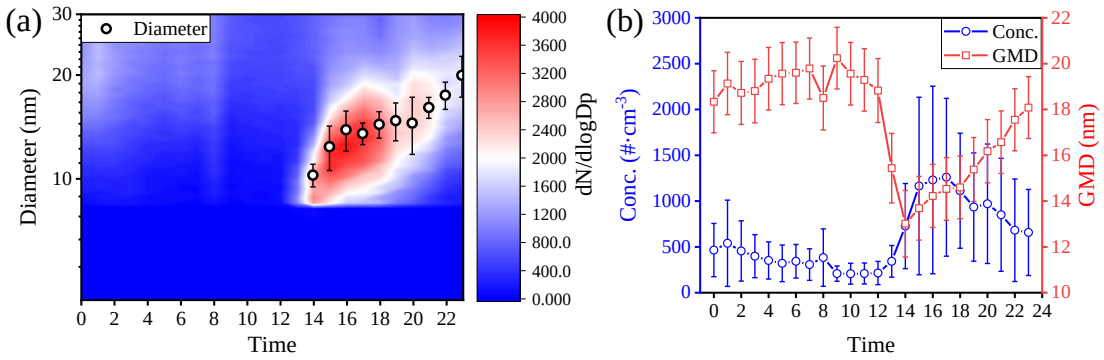

Figure 2 (a) The diurnal variation of PNSD for particle diameter is smaller than 30nm, and the contour from blue to red with the white intermediate color stands for the elevated number concentration $dN/d(\log Dp)$. In addition, the black circle with error bar is for the diameter corresponding to the maximum number concentration that was fitted

by lognormal function. (b) The diurnal variation of number concentration is presented by the blue circle with error bar, and the diurnal variation of GMD is plotted by the red square with error bar.

3.1.2 Atiken/accumulation mode

As known, particles with smaller diameter less than 30nm are less likely to be activated into a droplet unless they are under high supersaturation in the cloud process (Fan et al., 2018). Thus, it is necessary to observe the distribution characteristics of particles in Aitken and accumulation modes in order to estimate the activated critical diameter. In T2 period, particles ranging from 14.1 to 736.5nm in the alpine area were observed by using long-DMA from Jan. 9th to 23rd, 2021 (Figure S3). As shown in Figure S3, four episodes were divided corresponding to the PNSD during the sampling period: (1) P1 (Jan. 9th to 11th, 2021) and P4 (Jan. 19th to 23rd, 2021), without number concentration surge for particles with a diameter less than 30nm; (2) P2 (Jan. 11th to 13th, 2021) with dramatic increase concentration for particle around 30nm in diameter; (3) P3 (Jan. 14th to 18th, 2021) with the bimodal distribution occurred frequently. The variation of meteorological conditions was also different with each other in the four episodes, as shown in Figure S4. For example, temperature was low but relatively stable, while the relative humidity showed a gradually increasing trend in P1 episode. In P2 episode, while the temperature rose rapidly with large wind speed from southwest direction, the relative humidity and air pressure showed the opposite trend. In P3 cycle, the temperature decreased rapidly to -23℃ due the cold air mass and returned to normal temperature rapidly, while the relative humidity and pressure showed profiles of increasing first and then decreasing. The temperature was relatively high and accompanied by small fluctuations in P4 episode.

The diurnal mean variations of PNSD in the four episodes are shown in Figure 3. During P1 episode, the relative high number concentration spaned continuously from Aitken mode to the accumulation mode (Figure 3a). It was found from Figure 3b that the number concentration at night was significantly higher than that during the day, but the GMD was almost unchanged about 80 nm. While for P2 episode, most of particle were distributed in the diameter range of 20nm to 40nm with the maximum concentration of around 30nm, lying in the modes of nucleation and Aitken (Figure 3c). The number concentration was becoming smaller gradually along with GMD of particles becoming larger from 1:00 am to 13:00 pm (Figure 3d). Although the particle

417 in P3 episode (Figure 3e) was more extensive than the first two episodes, the relative
418 high number concentrtion stretch over the nucleation, Atiken and accumulation modse
419 range during the nighttime. In addition, the particles showed a bimodal distribution
420 pattern, and the two peaks gradually approached and merged into a single peak
421 distribution from the midday to the next dawn. The number concentration presented a
422 tendency for night to be higher than day value for first three episodes. The GMD
423 decreased and the number concentration increased from 13:00 to 18:00 p.m., which was
424 related to the intense photochemical reaction. As for P4, the number concentration
425 presented a tendency for day to be higher than night value in the accumulation mode,
426 which might be due to the shift of the source direction of the air mass (Figure 3g and
427 Figure S5). It could be concluded from Figure 3h that the increasing GMD tended to
428 decrease fleetly due to disturbances during the generation of new particle bursts.
429 However, it was obvious that the number concentration was almost the same with a
430 value of about 2000 #·cm^{-3}.

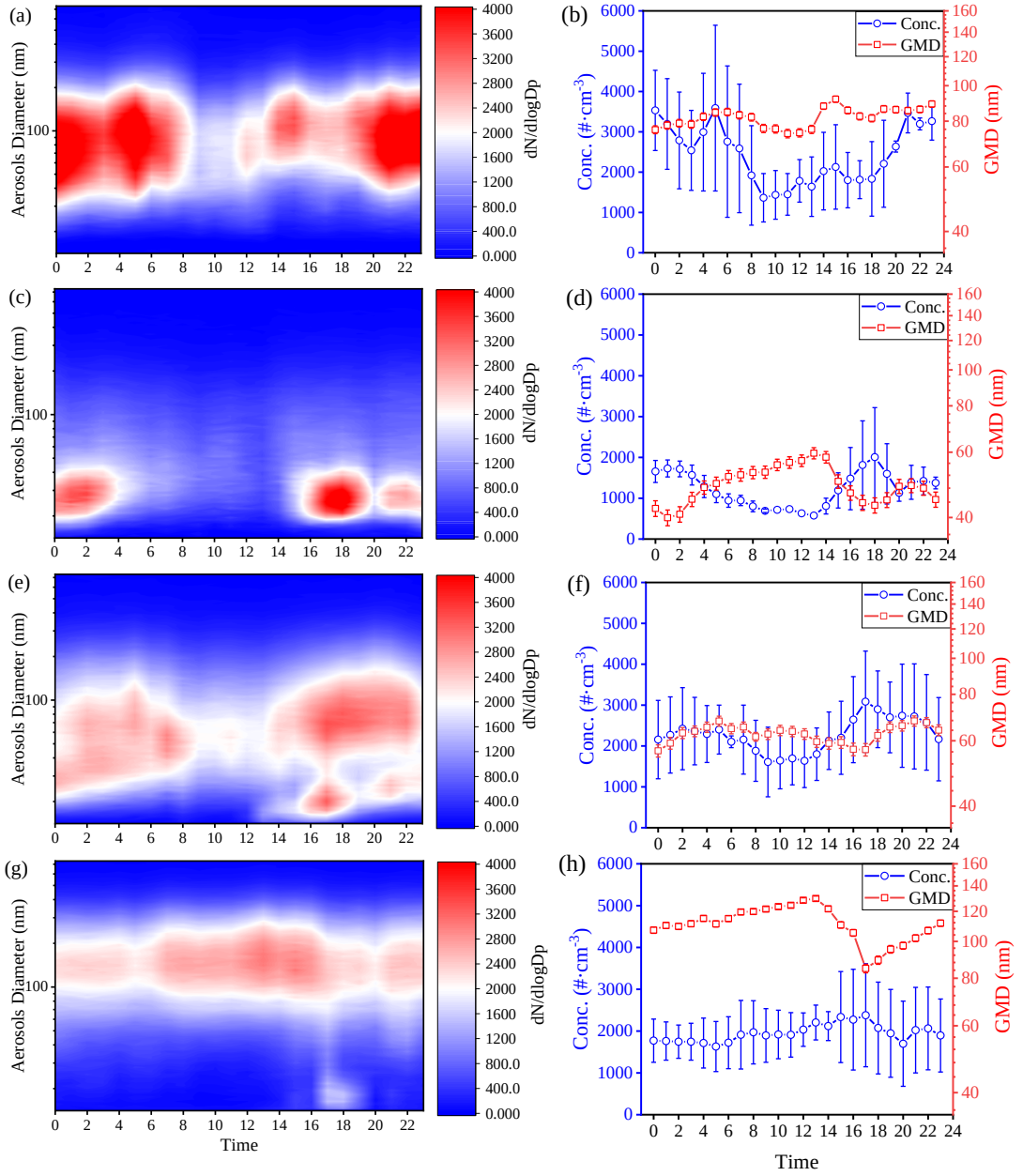

Figure 3 The diurnal *d*N/*d*(logDp) contour of PNSD for particle aerodynamic diameter and the number concentration for the second phase on the left panel. And the diurnal variation of number concentration is presented by the blue circle with error bar, and the diurnal variation of GMD is plotted by the red square with error bar on the right panel. What's more, the corresponding diagram of the specified measurement period is as follows: (a) and (b) for P1 period (9th Jan. to 11th Jan. 2021); (c) and (d) for P2 period (11th Jan. to 13th Jan. 2021); (e) and (f) for P3 period (14th Jan. to 18th Jan. 2021); (g) and (h) for P4 period (19th Jan. to 23rd Jan. 2021).

3.2 Correlation of PNSD with meteorological parameters and gaseous pollutants

3.2.1 Nucleation mode

As shown in Table S3, the average ambient temperature, relative humidity (RH) and wind speed during T1 period were -4.95±4.12℃, 41.52±17.52%, and 4.90±2.35 m/s, respectively. The prevailing wind direction were southwest and northwest (Figure S4).

As for T1 episode, in this study, the particle growth was positively correlated with RH (R=0.54), and negatively correlated with temperature (R=-0.32) (Table 1). In general, the synergistic effect of declining temperature and elevating RH would modulate the evolutionary growth and distribution of aerosol particles in the air. For example, on Dec. 23rd, 2020 the increasing RH and decreasing temperature were conducive to the formation of large particles, which resulted in no surge of the number concentration of particles with the size less than 30nm. Compared to the correlation between particle size and RH, however, the correlation between number concentration and RH showed the opposite trend (-0.22) in T1 episode (Kumar et al., 2011; Li et al., 2017b; Lyubovtseva et al., 2008), implying that particles in nucleation mode could adsorb water vapor in the environment and grow into particles with a larger particle size. There was no obvious correlation between temperature and number concentration in nucleation mode, indicating that it was not temperature that caused the explosion of number concentration, but photochemical reaction caused by strong solar radiation leading to the decreasing GMD. Thus, there was a negative correlation between elevating temperature and decreasing GMD. In addition, wind speed negatively correlated with number concentration (R=-0.33) and positively correlated with particle size (R=0.28), implying that higher wind speed could dilute the concentration of particles and to promote the growth of particles in nucleation mode.

Particle growth also depended significantly on the concentration of gaseous precursors in the atmosphere. For instance, the higher concentration of O_3 was favorable for the photochemical reaction to form new smaller particles and increase the concentration of particles (Baalbaki et al., 2021; Hara et al., 2021; Huang et al., 2021; Qi et al., 2015; Ueda et al., 2016). Wang et al. pointed out that enhanced formation of sulfate and SOA driven by photochemical oxidation could promote the formation and growth of new particles (Wang et al., 2016). Thus, O_3 had a positive correlation with particle number concentration (R=0.23) and a negative correlation with GMD (R=-0.36) in T1 episode. Furthermore, both SO_2 and NH_3 had positive correlation with GMD and negative correlation with number concentration, meaning that SO_2 and NH_3 had synergistic effect to accelerate the evolution of particles accompanied by the decrease

of number concentration (Berndt et al., 2008; Chu et al., 2016).

Table 1 the relationship of GMD and the number concentration with the meteorological parameters:RH, temperature, and wind speed, as well as the gaseous pollutants: O_3, CO, SO_2, and NH_3.

Coefficient (R)	GMD					Num. Conc.				
	T1	P1	P2	P3	P4	T1	P1	P2	P3	P4
RH	0.54**	0.60**	-ns	0.41**	0.84**	-0.22**	-ns	0.37*	0.52**	0.59**
Temp.	-0.32**	-0.30*	0.35*	-0.20*	-0.27**	-ns	-0.44**	-0.66**	-0.26**	-0.44**
WS	0.28**	0.36**	-ns	-ns	-0.27**	-0.33**	-ns	0.31*	-0.44**	-0.48**
O_3	-0.36**	-0.54**	-ns	-0.29**	0.61**	0.23**	-0.80**	-ns	-0.47**	0.33**
SO_2	0.45**	0.66**	-ns	0.36**	0.47**	-0.53**	0.77**	0.55**	0.66**	0.81**
NH_3	0.29**	0.53**	-ns	0.27**	0.64**	-0.2*	0.63**	-0.48**	0.33**	0.81**

ns: $p > 0.05$; *: $p < 0.05$; **: $p < 0.01$.

3.2.2 Aitken/accumulation mode

Table 1 summarizes the linear correlation of particle size and number concentration with meteorological parameters in T2 period. Meteorological parameters are shown in Table S3 in the supplementary. RH was recognized as one of the crucial meteorological factors positively affecting the GMD, supported by the larger particle size, the stronger the correlation for P1, P3, and P4 episodes. In addition, RH would promote the increase of number concentration in P2, P3, and P4 episodes. The increasing wind speed and RH had little effect on the number of particles in P1 episode, both of which had a greater impact on the particle size. While in P2 episode, it was reversed with P1 episode, that was, the wind speed and RH had a great effect on number concentration due to the gale wind ($12.6\pm2.4 m\cdot s^{-1}$) and lower RH ($18.4\pm4.7\%$), which was not conducive to the hygroscopic growth of particles. Wind speed was negatively correlated with particle size and number concentration in P3 and P4 episodes, meaning that the increase of wind speed was conducive to the removal of larger particles, leading to the reduction of GMD. However, in P2 episode, the gale wind removed large particles, which was conducive to the outbreak of number concentration with smaller diameter. As for the smaller size particles left behind in P2 episode after the larger diameter particles were blown away by higher wind speed, temperature ranked to be the most significant influence factor for GMD increasing, but temperature will reduce the GMD in other episodes. Moreover, temperature presented the negative correlation with number concentration for other

497 episodes. The reason was that the lower temperature was not conducive to the
498 condensation of gaseous molecules into clusters to increase the number of particles, nor
499 to the adsorption on the surface of existing particles to increase GMD. In addition, the
500 elevated temperature on the Mt. Hua was conducive to the diffusion of particles to
501 reduce the number concentration, for example, the negative correlation was -0.66
502 between number concentration and elevated temperature in P2 episode. In the published
503 literatures, when the temperature was lower than 0℃ in winter, the number
504 concentration showed a downward trend with the increase of temperature (Hussein et
505 al., 2006; Paasonen et al., 2013; Scott et al., 2017).

506 In P1 and P3 episodes when lager particles were more abundant and temperature
507 was lower, O_3 played the negative roles to GMD and number concentration. However,
508 O_3 presented a facilitation relationship with GMD and number concentration in P2 and
509 P4 episodes when temperatures was relatively higher. It could be interpreted that O_3
510 was able to oxidize the gaseous precursor to form solid or semi-solid matters at relative
511 high temperature, however, O_3 mainly reacted on the particle surface or in the bulk at
512 low temperature to consume the substances in the particles (Huang et al., 2021). Besides,
513 effects of SO_2 and NH_3 were significantly on GMD and number concentration of
514 particulate matter in P1, P3, and P4 episodes, indicating that they played a crucial role
515 in the growth process of particulate matter (Chu et al., 2016; He et al., 2021; Yang et
516 al., 2021). In P2 episode, however, the effects of the SO_2 on number concentration and
517 GMD were different, suggesting that the SO_2 played an important role in the formation
518 of particles to increase the number concentration rather than their diamter gowth. This
519 was consistent with the study of formation of granular seeds after SO_2 was converted
520 into sulfuric acid (Okuljar et al., 2021; Williamson et al., 2021; Zhao et al., 2021). In
521 addition, there was a negative correlation between NH_3 and number concentration due
522 to the low RH and the low concentration of NH_3.

523 **3.3 Characteristic of activated CCN**

524 Five supersaturations (SSs), i.e., 0.2%, 0.4%, 0.6%, 0.8%, and 1.0%, were set to
525 measure the N_{CCN} (Figure S6). The diurnal variation profiles of N_{CCN} for four episodes

526 in T2 were depicted in Figure 4. For the activated CCN particles, the diurnal variation
527 pattern was consistent with the change of aerosol number concentration. For P1, the
528 N_{CCN} decreased from 5:00 am until it reached the lowest number concentration at 9:00
529 am, and then showed an overall upward trend, resulting in the N_{CCN} at night being
530 significantly higher than that during the day. As the supersaturation increased from 0.2%
531 to 1.0%, the increase of aerosol number concentration did not show a linear positive
532 proportion, i.e., the difference of particle number concentration between two adjacent
533 supersaturations gradually decreased. The minimum number of activated N_{CCN} for P2
534 episode decreased from 3:00 am to 13:00 pm. In addition, the activated N_{CCN} did not
535 increase significantly with the increase of supersaturation, because the particles were
536 mainly distributed at the nucleation mode and part of Atiken mode with a low
537 probability of being activated at low supersaturation. However, N_{CCN} increased
538 obviously from 13:00 to 18:00 pm, meaning that the number concentration of particles
539 that can be activated in Aitken mode increased. It turned out that the products were
540 increased due to the enhanced photochemical reaction and subsequently adsorbed on
541 the surface of small diameter particles in the original or NPF event, resulting in the
542 larger particle diameter that can be activated when the diameter exceeded the critical
543 diameter. This indicated that the NPF events and their growth can affect the activated
544 N_{CCN}. This conclusion was also reported in previous studies (Eleftheriadis et al., 2020;
545 Kerminen et al., 2018; Rejano et al., 2021; Wu et al., 2017). During the P3 episode,
546 N_{CCN} also showed a trend of first decrease from 7:00 am to 14:00 pm and then increase
547 to 21:00 pm. It is worth noting that the activated particle number concentration showed
548 different patterns with supersaturation at diurnal profiles. For example, the different
549 from the diurnal variation of the number concentration of particles, the increased N_{CCN}
550 started from 14:00 to 21:00pm, rather than from 12: 00-17:00pm for aerosols.
551 Compared to other times, the difference between the activated number concentration
552 during this period at the same supersaturation gradually increased. For the P4 episode,
553 the concentration of activated particles from 5:00 am continued to increase until 15:00
554 pm due to the broaden lognormal distribution and the increased maxmum number
555 concentration leading to more N_{CCN}. However, the N_{CCN} showed the decreasing

tendency after 15:00 pm because of the narrowing lognormal distribution and the reduction of the maxmum number concentration, resulting in the less N_{CCN}. When the supersaturation exceeds 0.4% during this episode, the activated particle number concentration changed a little, meaning that the activated critical particle size of particles did not decrease gradual with the increase of supersaturation. It can be inferred that the hygroscopictity parameter of aerosol will gradually decrease with the supersatiration based on the Eq(6).

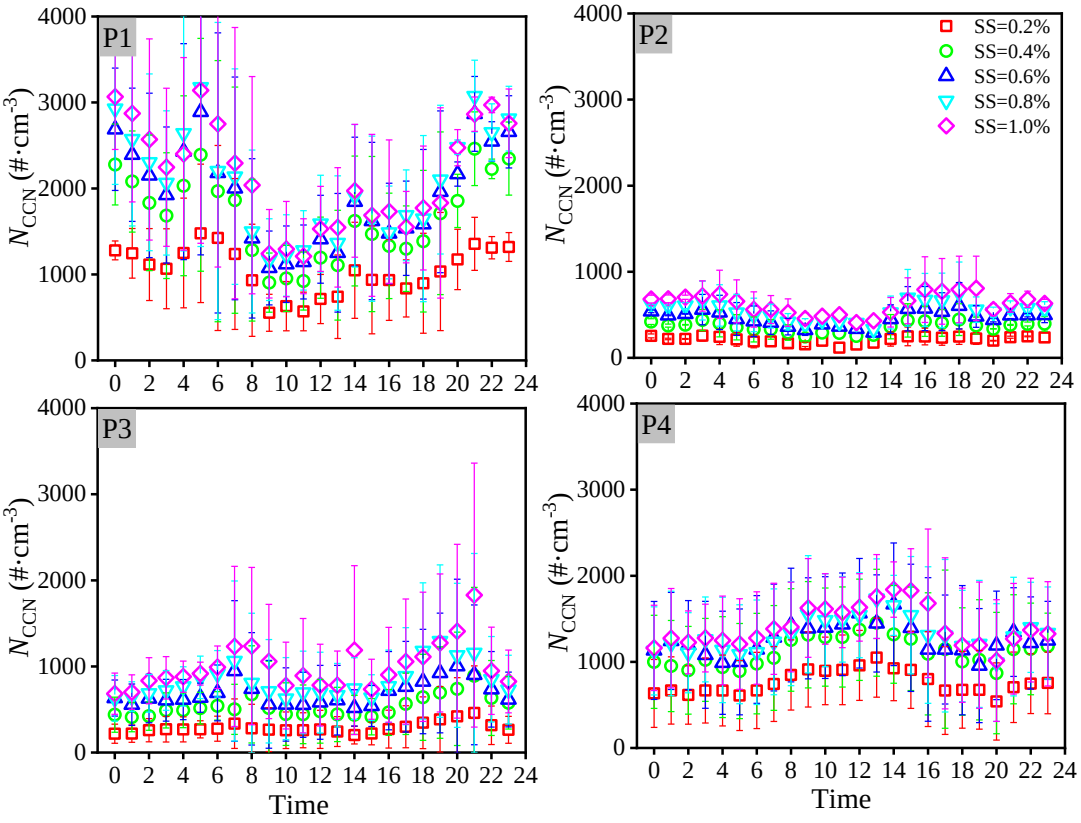

Figure 4 The diurnal variation of N_{CCN} for four episodes (P1, P2, P3, and P4) with five supersaturations of 0.2%, 0.4%, 0.6%, 0.8%, and 1.0%.

In the three modes, the order of activation was accumulation mode, Aitken mode and nucleation mode according to the Köhler theory(Li et al., 2017a; Petters and Kreidenweis, 2007). The number concentration of diurnal cycle of different mode of particles and NCCN when the supersaturation was 0.2% and 1.0%, respectively, were shown as Figure 2. When the supersaturation was 0.2%, the number concentration of CCN was mainly derived from the accumulation mode in all these 4 episodes. However, when the supersaturation was 1.0%, the contribution of CCN come from the particles

in the full accumulation mode and part of Aitken mode. Thus, the contribution of particles from Aitken mode become larger when the supersaturation increase to a high value in the cloud processes (Arub et al., 2020; Manoj et al., 2021; Patel and Jiang, 2021; Rejano et al., 2021; Wang et al., 2014).

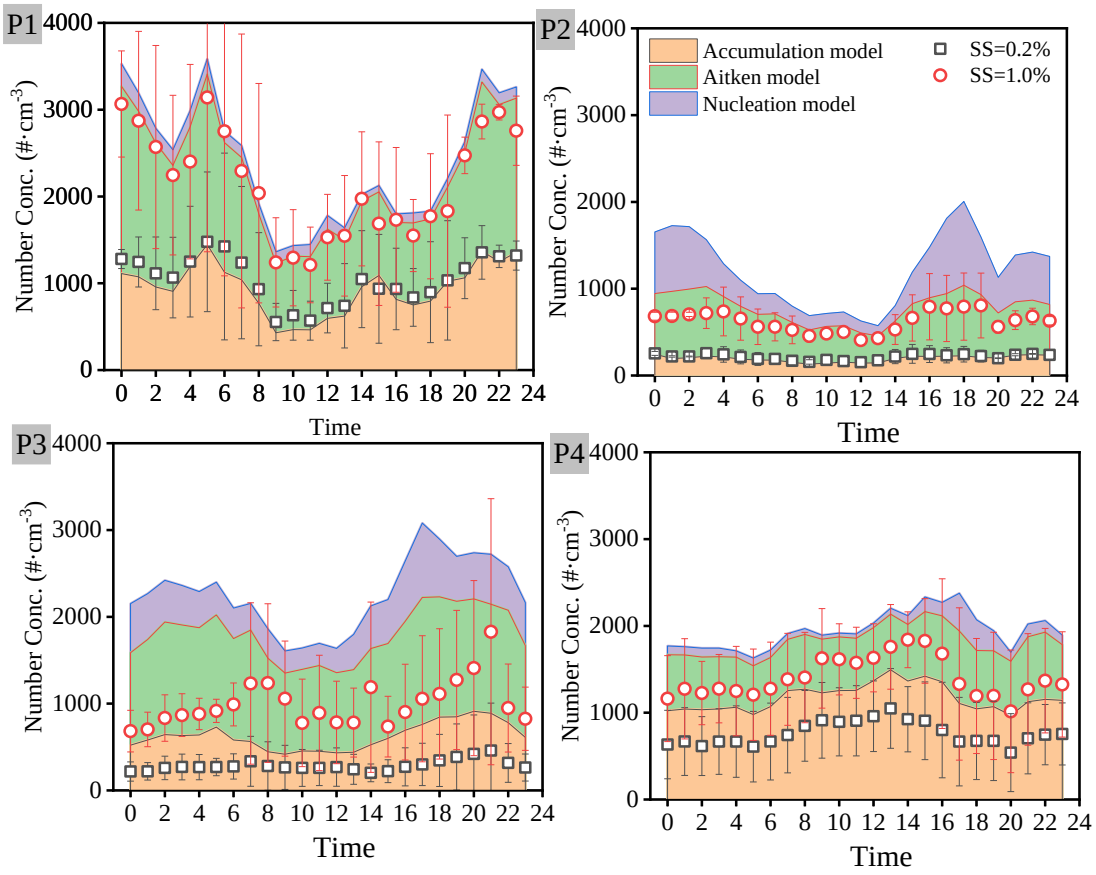

Figure 5 the diurnal cycle of different mode of particles and N_{CCN} when SS=0.2% and 1.0%, respectively.

3.4 Hygroscopicity and fitted two parameters

The combination measurements of PNSD and CCN activation distribution during nanoparticle events demonstrated the importance of the growth conversion from CCN aerosol particles to cloud droplets (O'Halloran et al., 2009). Subsequently, the critical particle size was calculated, that is, the ratio of the cumulative number concentration from the maximum particle size to the critical particle size to the total concentration was equal to the ratio of measured CCN/CN value. In addition, assuming that the

589 hygroscopic parameters, κ, are 0.1, 0.2, 0.3, 0.4, respectively, the corresponding critical
590 activated diameter values can be calculated, and the results were shown in the Figure
591 6(a). In P1 and P2 episodes, the critical dry particle diameter was distributed in Aitken
592 mode under 5 supersaturations, while it was mainly in accumulation mode in P3 when
593 the supersaturation was lower than 0.6%, and in P4 episodes when the supersaturation
594 was lower than 0.4%. With the increase of supersaturation, the critical size of the
595 activated particles becomes smaller. Interestingly, the critical particle diameter was
596 always larger than 30 nm of the upper limitation of nucleation mode division when the
597 supersaturation was below 1.0%, meaning that particles in the nucleation mode cannot
598 act as CCN to be activated into droplets in the mountain alpine area. The influence of
599 κ value is apparent on the critical particle size, that is, the larger its value is, the stronger
600 the hygroscopic capacity is, resulting in the activation of smaller diameter particles
601 (Dusek et al., 2010; Swietlicki et al., 2017). Under different supersaturation, predictions
602 for the lower limitation activated particle diameter calculated in P1 and P2 episodes
603 were in good agreement with the hygroscopicity parameters κ=0.4 and 0.3, respectively.
604 However, the critical diameter in P3 and P4 episodes was higher than the corresponding
605 value when κ=0.1, which meant that the hygroscopicity parameter of the actual particles
606 is less than 0.1 (Hung et al., 2016).
607

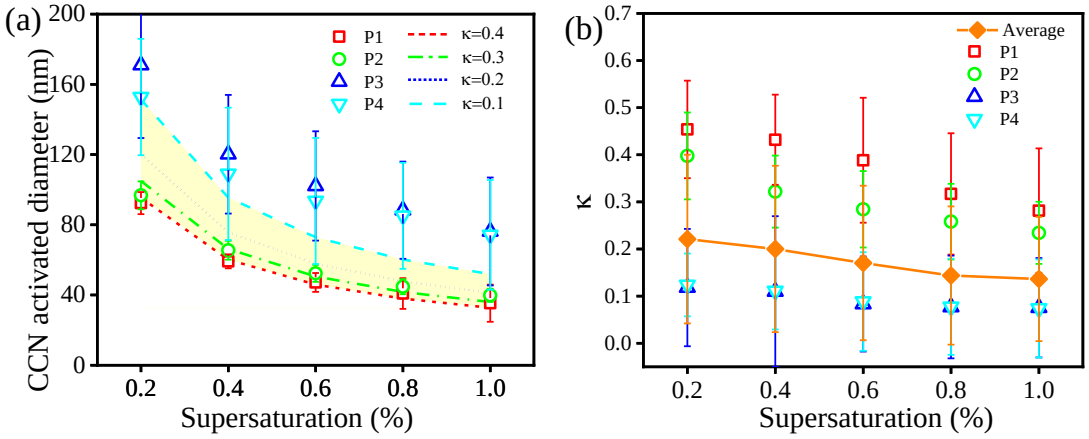

608
609 Figure 6 (a) critical activation particle size with supersaturation in four classification periods. The
610 lines stand for the CCN activated diameter with the supersaturation assuming that κ=0.1, 0.2, 0.3,
611 and 0.4. (b) the variation of κ with supersaturation for four periods and the orange diamond solid
612 dotted with line is for the entire measurement period.

613 Petters et al. fitted observations to a one-parameter model, where κ represented a

quantitative measure of aerosol water uptake characteristics and CCN activity (Petters and Kreidenweis, 2007). κ value could be obtained for each scenario with the prediction of the critical CCN particle size from PNSD based on the Eq. (6). Figure 6(b) depicted the κ value in each episode and the mean value of the whole measurement period. The average hygroscopicity parameters of the whole period at supersaturation of 0.2%, 0.4%, 0.6%, 0.8%, and 1.0% were 0.22, 0.20, 0.17, 0.14, and 0.13, respectively. Moreover, it can be inferred from Figure 6(b) that the hygroscopicity parameters showed a downward trend with the increase of supersaturation, which may be due to the dissolution of more less hygroscopic substances, such as less-hygroscopic organic matter and nearly hydrophobic carbon black in the bulk of smaller particle (Dusek et al., 2010; Swietlicki et al., 2017). κ value in P1 and P2 episodes were obviously larger than that in P3 and P4 (Figure 6(b)), which may be related to the air masses transport. As shown in Figure S5, air mass trajectories during P1 and P2 episodes mainly come from the northwest with a long-distance transportation, while in P3 and P4 episodes air masses did from local areas and gradually shift to the southwest.

Two parameter schemes, *C* and *k*, was adopted to fit the CCN spectral distribution, and the results were shown in Figure 7. High values of *C* parameter were typically found in polluted areas with high load of aerosol particles, while low values of *C* were characteristic for remote or background sites (Ji and Shaw, 1998; Rejano et al., 2021). In this study, the parameter *C* values were 2283#·cm^{-3}, 655#·cm^{-3}, 1139#·cm^{-3}, and 1488#·cm^{-3} corresponding to P1, P2, P3, and P4 episodes, respectively, which indeed was relative lower than that in polluted urban areas (Table S4). Moreover, the concentration of aerosol load measured at high altitude is lower than that on the ground (Varghese et al., 2016). The parameter *k* indicates the nature of the particles in terms of particle activation and takes values from 0.3 to 1.2, depending on the site-specific aerosol characteristics (Rejano et al., 2021). The values of *k* were 0.45, 0.67, 0.71, and 0.35 in the four periods in T2, respectively, which falled within the range proposed by previous studies (Hegg et al., 1991; Rejano et al., 2021).

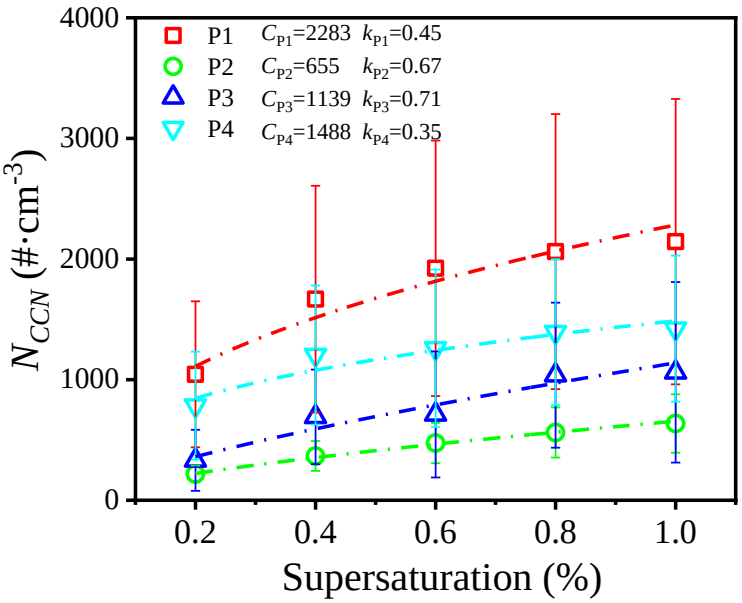

Figure 7 Variation of CCN number concentrations from 0.2 to 1.0% supersaturations on Mt. Hua.

It could be found from the two parameters that the C fitted from N_{CCN} was in the order of P1>P4>P3>P2, implying that the pollution caused by aerosols in P1 episode was the most serious, while in P2 episode was the least. The lower k value in P1 and P4 episodes indicated that the fitted CCN spectrum was relatively flat, and it could be inferred that the aerosol population dominated by hygroscopic or big aerosol particles in these two episodes. Through the PNSD and hygroscopicity parameter, it can be found that the higher hygroscopicity parameter was displayed in P1 episode, while the larger particle size of aerosols was expressed in P4 episode. On the contrary, the larger k value in P2 and P3 episodes indicated that the fitted CCN spectrum is steep, which were related to hydrophobic or ultrafine particles in these two episodes. The larger k value was consistent with the small aerosol particles in P2 episode, while the less hygroscopicity was for P3episode.

3.5 Predictions of N_{CCN} from PNSD measurements

Finally, the activation number concentration based on the average hygroscopicity parameter is compared with the measured number concentration to verify whether the average value can represent the hygroscopicity of Alpine aerosol. The N_{CCN}(PNSD) was calculated by the integral of the number concentration from critical particle diameter to the maximum particle diameter in the PNSD spectrum. The correlation and linear slope between the calculated N_{CCN}(PNSD) and the measured N_{CCN} are shown in Figure 8.

When the predicted N_{CCN} was higher than the measured one, the average κ value calculated by PNSD spectrum will be higher than the actual κ. That is, when the average calculated κ value was greater than the actual one, the number concentration of the activated particle was overestimated by PNSD spectrum. On the contrary, the number concentration of activated particles will be underestimated. Even if the average value was used to recalculate the number of activated particles, the concentration will be overestimated or underestimated. For example, it was slightly underestimated by 1% for 0.2% and 0.4% supersaturation, while for other supersaturations, it was marginally overestimated by 3%, 2%, and 2%, respectively. This small estimation error can be well accepted, so it was determined that the hygroscopicity of aerosol at the top of Mt. Hua was in the range of 0.13-0.22 with the supersaturation from 0.2-1.0%.

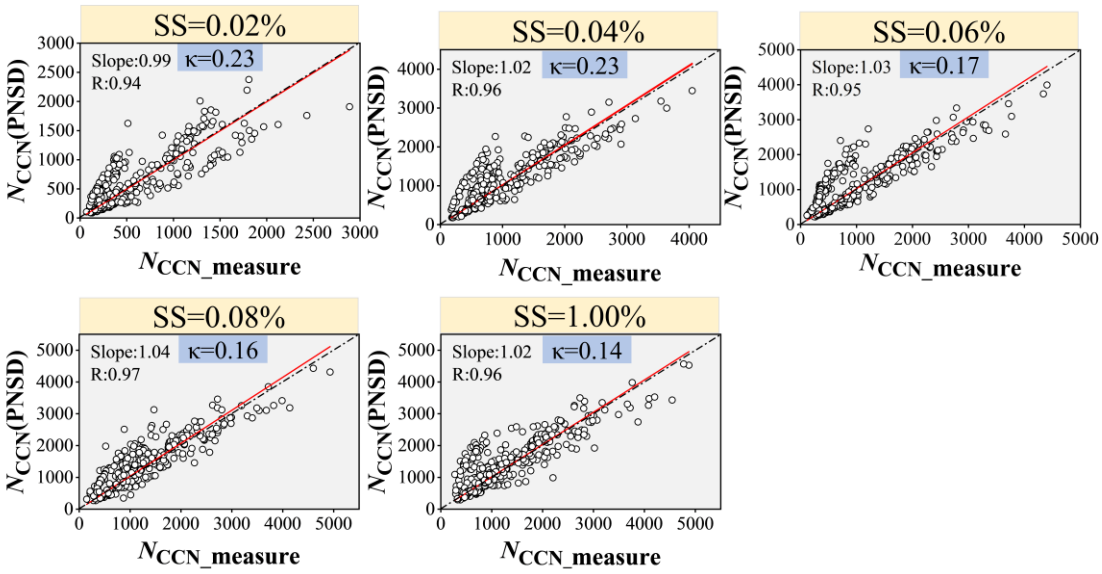

Figure 8 the calculated N_{CCN}(PNSD) vs. the measured N_{CCN} at different supersaturations from 0.2-1.0% with the average κ calculated by Eq. (6). The dot dash line was for 1:1 line and the red solid line was for the fitting curve.

4. Conclusion and Prospect

In this study, observation of PNSD and N_{CCN} were taken on the summit of the west peak of Mt. Hua over the period from Dec. 16th 2020 to Jan. 23rd for winter campaign. The number concentration of nucleation mode type particles with diameter smaller than 30nm erupted frequently from 13:00 to 18:00 p.m. due to the intense photochemistry in relative steady state meteorological conditions with the growth rate of 0.83nm·h^{-1}

lower than that of ground and urban measurement. Its diameter increased from nucleation mode of PSND and then merged into a single modal distribution of particles with larger particle size. In addition, the aerosol gradually increased in the daytime as the source direction of the air mass gradually shifted from northwest to southwest. The distribution characters of aerosol also varied with the meteorological conditions and gaseous pollutants. Moreover, RH has reverse effect on the increased trend of particle diameter and number concentration when it comes to the comparison of temperature influence. And the gale wind blow away the large diameter particles leaving smaller particles behind. On the other hand, SO_2 and NH_3 had a synergistic effect to contribute to the increase of particle diameter and number concentration for the relative larger suspended particle with positive correlation coefficient, but NH_3 had inverse effect on the number concentration for the nucleation mode particles. In addition, the influence of O_3 on the distribution characteristics of particle may be regulated by temperature. In the future research, the formation and growth mechanism of new particles can be accurately obtained through in-depth analysis of the chemical components of particles.

The load of N_{CCN} was lower on Mt. Hua compared to other regions such as urban and heavy polluted aera. And with the increase of supersaturation, more and more particles with smaller diameter were acted as CCN to be activated into droplets. Furthermore, the explosive increase of the nucleation mode particle and smaller Aitken mode particles can not act as CCN to be activated into droplets, but they have the potential to adsorb or absorb the polluted gaseous to promote the growth conversion into CCN, whose variation trend of the diurnal activated concentration is consistent with that of aerosol. In addition, the larger (P4)or more hygroscopic (P1) particles presented a small k value for the flat CCN spectra with the variation of supersaturation, while the ultrafine (P2) or hydrophobic (P3) particles presented a relative larger k value for the steep CCN spectra. Still further, hygroscopicity parameters, which may be affected by more insoluble substances or organic components dissolved in droplets due to the gradual shift of air mass source from northwest to southwest, show a downward trend with the increase of supersaturation. Ultimately, with the small deviation betweent the calculated from PNSD and the measured N_{CCN}, it can be inferred undoubtedly that the average

hygroscopicity parameter of particles on Mt. Hua decreases from 0.22 to 0.13 with the supersaturation from 0.2 to 1.0%. Thus, the interaction between aerosol and cloud can be estimated more accurately than that on ground measurement and the uncertainty of indrect effect will be shrinked than ever before.

Acknowledgments

This work was financially supported by the program from National Natural Science Foundation of China (No. 41977332), the Strategic Priority Research Program of Chinese Academy of Sciences (No. XDB40000000). Jianjun Li also acknowledged the support of the Youth Innovation Promotion Association CAS (No. 2020407). We thank the meteorological station of Huashan for providing the sampling site and meteorological datas, as well as its staffs for their help. Our acknowledgment also goes to the State Key Laboratory of Multiphase Flow in Power Engineering of Xi'an Jiaotong University and Key Lab of Aerosol Chemistry and Physics of IEECAS for providing SMPS, CCN and gaseous pollutants analyzers. The authors would like to express gratitude to the anonymous reviewers who supplied valuable feedback toward improving this manuscript.

Conflict of Interest

The authors declare no conflicts of interest relevant to this study

Open Research

Data Availability Statement

Datasets for this research are included in this paper (and its supplementary information files): The ERA5 reanalysis data used for boundary layer height and surface net solar radiation in supplementary information file are available on the website of https://cds.climate.copernicus.eu/cdsapp#!/dataset/reanalysis-era5-single-levels-monthly-means?tab=form (Bell et al., 2021; Hersbach et al., 2020). HYSPLIT model can run online from NOAA Air Resources Laboratory website (https://www.ready.noaa.gov/HYSPLIT_traj.php) without register (Rolph et al., 2017; Stein et al., 2015). Data presented in this paper (and its supplementary information files) are freely accessible from the following link: https://zenodo.org/record/62476664#.YmIKjoVByUk

References:

Andreae, M. O., Andreae, T. W., Ditas, F., & Pöhlker, C. (2022). Frequent new particle formation at remote sites in the subboreal forest of North America. *Atmospheric Chemistry and Physics*, *22*(4), 2487-2505, http://doi.org/10.5194/acp-22-2487-2022.

Arub, Z., Bhandari, S., Gani, S., Apte, J. S., Hildebrandt Ruiz, L., & Habib, G. (2020). Air mass physiochemical characteristics over New Delhi: impacts on aerosol hygroscopicity and cloud condensation nuclei (CCN) formation. *Atmospheric Chemistry and Physics*, *20*(11), 6953-6971, http://doi.org/10.5194/acp-20-6953-2020.

Baalbaki, R., et al. (2021). Towards understanding the characteristics of new particle formation in the Eastern Mediterranean. *Atmospheric Chemistry and Physics*, *21*(11), 9223-9251, http://doi.org/10.5194/acp-21-9223-2021.

Babu, S. S., Kompalli, S. K., & Moorthy, K. K. (2016). Aerosol number size distributions over a coastal semi urban location: Seasonal changes and ultrafine particle bursts. *The Science of the total environment*, *563-564*, 351-365, http://doi.org/10.1016/j.scitotenv.2016.03.246.

Bell, B., et al. (2021). The ERA5 global reanalysis: Preliminary extension to 1950 [Dataset]. *Quarterly Journal of the Royal Meteorological Society*, http://doi.org/10.1002/qj.4174.

Berndt, T., Stratmann, F., Sipilä, M., Grüner, A., Spindler, G., & Kulmala, M. (2008). Influence of NH3 on atmospheric particle formation starting from OH + SO2. *European Aerosol Conference (EAC)*, Stick T06A053O.

Burkart, J., Steiner, G., Reischl, G., & Hitzenberger, R. (2011). Long-term study of cloud condensation nuclei (CCN) activation of the atmospheric aerosol in Vienna. *Atmos Environ (1994)*, *45*(32), 5751-5759, http://doi.org/10.1016/j.atmosenv.2011.07.022.

Cai, M., et al. (2021). The important roles of surface tension and growth rate in the contribution of new particle formation (NPF) to cloud condensation nuclei (CCN) number concentration: evidence from field measurements in southern China. *Atmospheric Chemistry and Physics*, *21*(11), 8575-8592, http://doi.org/10.5194/acp-21-8575-2021.

Cai, M., Tan, H., Chan, C. K., Qin, Y., Xu, H., Li, F., Schurman, M. I., Liu, L., & Zhao, J. (2018). The size-resolved cloud condensation nuclei (CCN) activity and its prediction based on aerosol hygroscopicity and composition in the Pearl Delta River (PRD) region during wintertime 2014. *Atmospheric Chemistry and Physics*, *18*(22), 16419-16437, http://doi.org/10.5194/acp-18-16419-2018.

Chang, D. Y., Lelieveld, J., Tost, H., Steil, B., Pozzer, A., & Yoon, J. (2017). Aerosol physicochemical effects on CCN activation simulated with the chemistry-climate model EMAC. *Atmospheric Environment*, *162*, 127-140, http://doi.org/10.1016/j.atmosenv.2017.03.036.

Charnawskas, J. C., et al. (2017). Condensed-phase biogenic-anthropogenic interactions with implications for cold cloud formation. *Faraday discussions*, *200*, 165-194, http://doi.org/10.1039/c7fd00010c.

Chen, L., Li, Q., Wu, D., Sun, H., Wei, Y., Ding, X., Chen, H., Cheng, T., & Chen, J. (2019). Size distribution and chemical composition of primary particles emitted during open biomass burning processes: Impacts on cloud condensation nuclei activation. *The Science of the total environment*, *674*, 179-188, http://doi.org/10.1016/j.scitotenv.2019.03.419.

Chen, X., Wang, Z., Li, J., Chen, H., Hu, M., Yang, W., Wang, Z., Ge, B., & Wang, D. (2017). Explaining the spatiotemporal variation of fine particle number concentrations over Beijing and surrounding areas in an air quality model with aerosol microphysics. *Environmental pollution*, *231*(Pt 2), 1302-1313, http://doi.org/10.1016/j.envpol.2017.08.103.

Chu, B., Zhang, X., Liu, Y., He, H., Sun, Y., Jiang, J., Li, J., & Hao, J. (2016). Synergetic formation of secondary inorganic and organic aerosol: effect of SO2 and NH3on particle formation and growth. *Atmospheric Chemistry and Physics*, *16*(22), 14219-14230, http://doi.org/10.5194/acp-16-14219-2016.

Dameto de España, C., Wonaschütz, A., Steiner, G., Rosati, B., Demattio, A., Schuh, H., & Hitzenberger, R. (2017). Long-term quantitative field study of New Particle Formation (NPF) events as a source of Cloud Condensation Nuclei (CCN) in the urban background of Vienna. *Atmospheric Environment*, *164*, 289-298, http://doi.org/10.1016/j.atmosenv.2017.06.001.

Deng, C., et al. (2020). Seasonal Characteristics of New Particle Formation and Growth in Urban Beijing. *Environmental science & technology*, *54*(14), 8547-8557, http://doi.org/10.1021/acs.est.0c00808.

Dusek, U., Covert, D. S., Wiedensohler, A., Neususs, C., Weise, D., & Cantrell, W. (2003). Cloud condensation nuclei spectra derived from size distributions and hygroscopic properties of the aerosol in coastal south-west Portugal during ACE-2. *Tellus B*, *55*(1), 35-53, http://doi.org/10.1034/j.1600-0889.2003.00041.x.

Dusek, U., Frank, G. P., Curtius, J., Drewnick, F., & Pöschl, U. (2010). Enhanced organic mass fraction and decreased hygroscopicity of cloud condensation nuclei (CCN) during new particle formation events. *Geophysical Research Letters*, *37*(3), http://doi.org/10.1029/2009GL040930.

Eleftheriadis, K., Gini, M., Mendes, L., Ondracek, J., Krejci, R., & Tørseth, K. (2020). Potential mechanisms for New Particle Formation and growth from aerosol mixing state and volatility observations. *EGU General Assembly 2020*, EGU2020-21798, http://doi.org/10.5194/egusphere-egu2020-21798.

Fan, J., et al. (2018). Substantial convection and precipitation enhancements by ultrafine aerosol particles. *Science*, *359*(6374), 411-418, http://doi.org/10.1126/science.aan8461.

Franco, M. A., et al. (2022). Occurrence and growth of sub-50 nm aerosol particles in the Amazonian boundary layer. *Atmospheric Chemistry and Physics*, *22*(5), 3469-3492, http://doi.org/10.5194/acp-22-3469-2022.

Gao, J., Chai, F., Wang, T., & Wang, W. (2011). Particle number size distribution and new particle formation (NPF) in Lanzhou, Western China. *Particuology*, *9*(6), 611-618, http://doi.org/10.1016/j.partic.2011.06.008.

Gao, J., Wang, T., Zhou, X., Wu, W., & Wang, W. (2009). Measurement of aerosol number size distributions in the Yangtze River delta in China: Formation and growth of particles under polluted conditions. *Atmospheric Environment*, *43*(4), 829-836, http://doi.org/10.1016/j.atmosenv.2008.10.046.

Gaston, C., Cahill, J., Collins, D., Suski, K., Ge, J., Barkley, A., & Prather, K. (2018). The Cloud Nucleating Properties and Mixing State of Marine Aerosols Sampled along the Southern California Coast. *Atmosphere*, *9*(2), http://doi.org/10.3390/atmos9020052.

Gogoi, M. M., Moorthy, K. K., Kompalli, S. K., Chaubey, J. P., Babu, S. S., Manoj, M. R., Nair, V. S., & Prabhu, T. P. (2014). Physical and optical properties of aerosols in a free tropospheric environment: Results from long-term observations over western trans-Himalayas. *Atmospheric Environment*, *84*, 262-274, http://doi.org/10.1016/j.atmosenv.2013.11.029.

Grainger, R. G. (2020). Some Useful Formulae for Aerosol Size Distributions and Optical Properties, edited, http://eodg.atm.ox.ac.uk/user/grainger/research/aerosols.pdf.

Hakim, Z. Q., Archer-Nicholls, S., Beig, G., Folberth, G. A., Sudo, K., Abraham, N. L., Ghude, S., Henze, D. K., & Archibald, A. T. (2019). Evaluation of tropospheric ozone and ozone precursors in simulations from the HTAPII and CCMI model intercomparisons – a focus on the Indian subcontinent. *Atmospheric Chemistry and Physics*, *19*(9), 6437-6458, http://doi.org/10.5194/acp-19-6437-2019.

Han, Y., Iwamoto, Y., Nakayama, T., Kawamura, K., Hussein, T., & Mochida, M. (2013). Observation of new particle formation over a mid-latitude forest facing the North Pacific. *Atmospheric Environment*, *64*, 77-84, http://doi.org/10.1016/j.atmosenv.2012.09.036.

Hara, K., Nishita-Hara, C., Osada, K., Yabuki, M., & Yamanouchi, T. (2021). Characterization of aerosol number size distributions and their effect on cloud properties at Syowa Station, Antarctica. *Atmospheric Chemistry and Physics*, *21*(15), 12155-12172, http://doi.org/10.5194/acp-21-12155-2021.

He, X., Wu, J.-J., Ma, Z.-C., Xi, X., & Zhang, Y.-H. (2021). NH3-promoted heterogeneous reaction of SO2 to sulfate on α-Fe2O3 particles with coexistence of NO2 under different relative humidities. *Atmospheric Environment*, *262*, http://doi.org/10.1016/j.atmosenv.2021.118622.

He, Y., Pan, Y., Zhang, G., Ji, D., Tian, S., Xu, X., Zhang, R., & Wang, Y. (2020). Tracking ammonia morning peak, sources and transport with 1 Hz measurements at a rural site in North China Plain. *Atmospheric Environment*, *235*, http://doi.org/10.1016/j.atmosenv.2020.117630.

Hegg, D. A., Radke, L. F., & Hobb, P. V. (1991). Measurements of Aitken nuclei and cloud condensation nuclei in the marine atmosphere and their relation to the DMS-cloudclimate hypothesis. *Journal of Geophysical Research Atmospheres*, *96*(D10), 18727-18733, http://doi.org/10.1029/91JD01870.

Hersbach, H., et al. (2020). The ERA5 global reanalysis [Dtaset]. *Quarterly Journal of the Royal Meteorological Society*, http://doi.org/10.1002/qj.3803.

Huang, X., et al. (2021). Enhanced secondary pollution offset reduction of primary emissions during COVID-19 lockdown in China. *National Science Review*, *8*(2), http://doi.org/10.1093/nsr/nwaa137.

Hughes, M., Kodros, J., Pierce, J., West, M., & Riemer, N. (2018). Machine Learning to Predict the Global Distribution of Aerosol Mixing State Metrics. *Atmosphere*, *9*(1), http://doi.org/10.3390/atmos9010015.

Hung, H.-M., Hsu, C.-H., Lin, W.-T., & Chen, Y.-Q. (2016). A case study of single hygroscopicity parameter and its link to the functional groups and phase transition for urban aerosols in Taipei City. *Atmospheric Environment*, *132*, 240-248, http://doi.org/10.1016/j.atmosenv.2016.03.008.

Hung, H.-M., Lu, W.-J., Chen, W.-N., Chang, C.-C., Chou, C. C. K., & Lin, P.-H. (2014). Enhancement of the hygroscopicity parameter kappa of rural aerosols in northern Taiwan by anthropogenic emissions. *Atmospheric Environment*, *84*, 78-87, http://doi.org/10.1016/j.atmosenv.2013.11.032.

Hussein, T., Karppinen, A., Kukkonen, J., Härkönen, J., Aalto, P. P., Hämeri, K., Kerminen, V.-M., & Kulmala, M. (2006). Meteorological dependence of size-fractionated number concentrations of urban aerosol particles. *Atmospheric Environment*, *40*(8), 1427-1440, http://doi.org/10.1016/j.atmosenv.2005.10.061.

Jayachandran, V., Nair, V. S., & Babu, S. S. (2017). CCN characteristics over a tropical coastal station during south-west monsoon: observations and closure studies. *Atmospheric Environment*, *164*, 299-308, http://doi.org/10.1016/j.atmosenv.2017.06.012.

Jayachandran, V., Nair, V. S., & Babu, S. S. (2018). CCN activation properties at a tropical hill station in Western Ghats during south-west summer monsoon: Vertical heterogeneity. *Atmospheric Research*, *214*, 36-45, http://doi.org/10.1016/j.atmosres.2018.07.018.

Ji, Q., & Shaw, G. E. (1998). On supersaturation spectrum and size distributions of cloud condensation nuclei. *Geophysical Research Letters*, *25*(11), 1903-1906, http://doi.org/10.1029/98gl01404.

Kammermann, L., Gysel, M., Weingartner, E., Herich, H., Cziczo, D. J., Holst, T., Svenningsson, B., Arneth, A., & Baltensperger, U. (2010). Subarctic atmospheric aerosol composition: 3. Measured and modeled properties of cloud condensation nuclei. *J Geophys Res-Atmos*, *115*(D4), http://doi.org/10.1029/2009jd012447.

Kanawade, V. P., Tripathi, S. N., Siingh, D., Gautam, A. S., Srivastava, A. K., Kamra, A. K., Soni, V. K., & Sethi, V. (2014). Observations of new particle formation at two distinct Indian subcontinental urban locations. *Atmospheric Environment*, *96*, 370-379, http://doi.org/10.1016/j.atmosenv.2014.08.001.

Kerminen, V.-M., Chen, X., Vakkari, V., Petäjä, T., Kulmala, M., & Bianchi, F. (2018). Atmospheric new particle formation and growth: review of field observations. *Environmental Research Letters*, *13*(10), http://doi.org/10.1088/1748-9326/aadf3c.

Kim, N., Park, M., Yum, S. S., Park, J. S., Shin, H. J., & Ahn, J. Y. (2018). Impact of urban aerosol properties on cloud condensation nuclei (CCN) activity during the KORUS-AQ field campaign. *Atmospheric Environment*, *185*, 221-236, http://doi.org/10.1016/j.atmosenv.2018.05.019.

Kim, N., et al. (2017). Hygroscopic properties of urban aerosols and their cloud condensation nuclei activities measured in Seoul during the MAPS-Seoul campaign. *Atmospheric Environment*, *153*, 217-232, http://doi.org/10.1016/j.atmosenv.2017.01.034.

Kompalli, S. K., Babu, S. S., Moorthy, K. K., Gogoi, M. M., Nair, V. S., & Chaubey, J. P. (2014). The formation and growth of ultrafine particles in two contrasting environments: a case study. *Annales Geophysicae*, *32*(7), 817-830, http://doi.org/https://doi.org/10.5194/angeo-32-817-2014.

Konovalov, I. B., Golovushkin, N. A., Beekmann, M., & Andreae, M. O., http://doi.org/10.5194/acp-2020-591.

Koponen, I. K. (2003). Number size distributions and concentrations of the continental summer aerosols in Queen Maud Land, Antarctica. *Journal of Geophysical Research*, *108*(D18), http://doi.org/10.1029/2003jd003614.

Kulmala, M., & Kerminen, V.-M. (2008). On the formation and growth of atmospheric nanoparticles. *Atmospheric Research*, *90*(2-4), 132-150, http://doi.org/10.1016/j.atmosres.2008.01.005.

Kulmala, M., et al. (2012). Measurement of the nucleation of atmospheric aerosol particles. *Nat Protoc*, *7*(9), 1651-1667, http://doi.org/10.1038/nprot.2012.091.

Kulmala, M., Vehkamäki, H., Petäjä, T., Dal Maso, M., Lauri, A., Kerminen, V. M., Birmili, W., & McMurry, P. H. (2004). Formation and growth rates of ultrafine atmospheric particles: a review of observations. *Journal of Aerosol Science*, *35*(2), 143-176, http://doi.org/10.1016/j.jaerosci.2003.10.003.

Kumar, A., Saxena, D., & Yadav, R. (2011). Measurements of atmospheric aerosol concentration of various sizes during monsoon season at Roorkee, India. *Atmospheric Science Letters*, *12*(4), 345-350, http://doi.org/10.1002/asl.347.

Lampilahti, J., et al. (2021). Zeppelin-led study on the onset of new particle formation in the planetary boundary layer. *Atmospheric Chemistry and Physics*, *21*(16), 12649-12663, http://doi.org/10.5194/acp-21-12649-2021.

Li, J., Wang, G., Zhou, B., Cheng, C., Cao, J., Shen, Z., & An, Z. (2011a). Chemical composition and size distribution of wintertime aerosols in the atmosphere of Mt. Hua in central China. *Atmospheric Environment*, *45*(6), 1251-1258, http://doi.org/10.1016/j.atmosenv.2010.12.009.

Li, J., et al. (2017a). Chemical composition and droplet size distribution of cloud at the summit of Mount Tai, China. *Atmospheric Chemistry and Physics*, *17*(16), 9885-9896, http://doi.org/10.5194/acp-17-9885-2017.

Li, J., et al. (2020). The evolution of cloud and aerosol microphysics at the summit of Mt. Tai, China. *Atmospheric Chemistry and Physics*, *20*(22), 13735-13751, http://doi.org/10.5194/acp-20-13735-2020.

Li, J. J., Wang, G. H., Cao, J. J., Wang, X. M., & Zhang, R. J. (2013). Observation of biogenic secondary organic aerosols in the atmosphere of a mountain site in central China: temperature and relative humidity effects. *Atmospheric Chemistry and Physics*, *13*(22), 11535-11549, http://doi.org/10.5194/acp-13-11535-

2013.

Li, K., Ye, X., Pang, H., Lu, X., Chen, H., Wang, X., Yang, X., Chen, J., & Chen, Y. (2018). Temporal variations in the hygroscopicity and mixing state of black carbon aerosols in a polluted megacity area. *Atmospheric Chemistry and Physics*, *18*(20), 15201-15218, http://doi.org/10.5194/acp-18-15201-2018.

Li, W., et al. (2014). Composition and hygroscopicity of aerosol particles at Mt. Lu in South China: Implications for acid precipitation. *Atmospheric Environment*, *94*, 626-636, http://doi.org/10.1016/j.atmosenv.2014.06.003.

Li, W. J., Zhang, D. Z., Shao, L. Y., Zhou, S. Z., & Wang, W. X. (2011b). Individual particle analysis of aerosols collected under haze and non-haze conditions at a high-elevation mountain site in the North China plain. *Atmospheric Chemistry and Physics*, *11*(22), 11733-11744, http://doi.org/10.5194/acp-11-11733-2011.

Li, X., Ma, Y., Wang, Y., Liu, N., & Hong, Y. (2017b). Temporal and spatial analyses of particulate matter (PM 10 and PM 2.5) and its relationship with meteorological parameters over an urban city in northeast China. *Atmospheric Research*, *198*, 185-193, http://doi.org/10.1016/j.atmosres.2017.08.023.

Li, Z., et al. (2019). East Asian Study of Tropospheric Aerosols and their Impact on Regional Clouds, Precipitation, and Climate (EAST-AIR$_{CPC}$). *Journal of Geophysical Research: Atmospheres*, *124*(23), 13026-13054, http://doi.org/10.1029/2019jd030758.

Liu, S., Hu, M., Wu, Z., Wehner, B., Wiedensohler, A., & Cheng, Y. (2008). Aerosol number size distribution and new particle formation at a rural/coastal site in Pearl River Delta (PRD) of China. *Atmospheric Environment*, *42*(25), 6275-6283, http://doi.org/10.1016/j.atmosenv.2008.01.063.

Lyubovtseva, Y. S., Sogacheva, L., & Kulmala, M. (2008). Variations of trace gases, meteorological parameters, and their connection with aerosol formation in boreal forests. *Russian Journal of Earth Sciences*, *10*(2), 1-4, http://doi.org/10.2205/2007es000260.

Ma, Y., Li, S., Zheng, J., Khalizov, A., Wang, X., Wang, Z., & Zhou, Y. (2017). Size-resolved measurements of mixing state and cloud-nucleating ability of aerosols in Nanjing, China. *Journal of Geophysical Research: Atmospheres*, *122*(17), 9430-9450, http://doi.org/10.1002/2017jd026583.

Mallet, M. D., Cravigan, L. T., Milic, A., Alroe, J., Ristovski, Z. D., Ward, J., Keywood, M., Williams, L. R., Selleck, P., & Miljevic, B. (2016). Composition, size and cloud condensation nuclei activity of biomass burning aerosol from north Australian savannah fires. *Atmospheric Chemistry and Physics Discussions*, 1-24, http://doi.org/10.5194/acp-2016-867.

Manoj, M. R., Satheesh, S. K., Moorthy, K. K., Trembath, J., & Coe, H. (2021). Measurement report: Altitudinal variation of cloud condensation nuclei activation across the Indo-Gangetic Plain prior to monsoon onset and during peak monsoon periods: results from the SWAAMI field campaign. *Atmospheric Chemistry and Physics*, *21*(11), 8979-8997, http://doi.org/10.5194/acp-21-8979-2021.

Martin, N. A., Ferracci, V., Cassidy, N., & Hoffnagle, J. A. (2016). The application of a cavity ring-down spectrometer to measurements of ambient ammonia using traceable primary standard gas mixtures. *Appl Phys B-Lasers O*, *122*(8), http://doi.org/10.1007/s00340-016-6486-9.

Miao, Q., Zhang, Z., Li, Y., Qin, X., Xu, B., Yuan, Y., & Gao, Z. (2015). Measurement of cloud condensation nuclei (CCN) and CCN closure at Mt. Huang based on hygroscopic growth factors and aerosol number-size distribution. *Atmospheric Environment*, *113*, 127-134, http://doi.org/10.1016/j.atmosenv.2015.05.006.

Minoura, H., & Takekawa, H. (2005). Observation of number concentrations of atmospheric aerosols and analysis of nanoparticle behavior at an urban background area in Japan. *Atmospheric Environment*, *39*(32), 5806-5816, http://doi.org/10.1016/j.atmosenv.2005.06.033.

Mönkkönen, P., Koponen, I. K., Lehtinen, K. E. J., Hämeri, K., Uma, R., & Kulmala, M. (2005). Measurements in a highly polluted Asian mega city: observations of aerosol number size distribution, modal parameters and nucleation events. *Atmospheric Chemistry And Physics*, *5*, 57-66, http://doi.org/10.5194/acp-5-57-2005

Monteiro dos Santos, D., Rizzo, L. V., Carbone, S., Schlag, P., & Artaxo, P. (2021). Physical and chemical properties of urban aerosols in São Paulo, Brazil: links between composition and size distribution of submicron particles. *Atmospheric Chemistry and Physics*, *21*(11), 8761-8773, http://doi.org/10.5194/acp-21-8761-2021.

O'Halloran, T. L., Fuentes, J. D., Collins, D. R., Cleveland, M. J., & Keene, W. C. (2009). Influence of air mass source region on nanoparticle events and hygroscopicity in central Virginia, U.S. *Atmospheric Environment*, *43*(22-23), 3586-3595, http://doi.org/10.1016/j.atmosenv.2009.03.033.

Okuljar, M., et al. (2021). Measurement report: The influence of traffic and new particle formation on the size distribution of 1–800 nm particles in Helsinki – a street canyon and an urban background station comparison. *Atmospheric Chemistry and Physics*, *21*(13), 9931-9953, http://doi.org/10.5194/acp-21-9931-2021.

Paasonen, P., et al. (2013). Warming-induced increase in aerosol number concentration likely to moderate climate change. *Nature Geoscience*, *6*(6), 438-442, http://doi.org/10.1038/ngeo1800.

Patel, P. N., & Jiang, J. H. (2021). Cloud condensation nuclei characteristics at the Southern Great Plains site: role of particle size distribution and aerosol hygroscopicity. *Environmental Research Communications*, *3*(7), http://doi.org/10.1088/2515-7620/ac0e0b.

Peng, C., et al. (2020). Tropospheric aerosol hygroscopicity in China. *Atmospheric Chemistry and Physics*, *20*(22), 13877-13903, http://doi.org/10.5194/acp-20-13877-2020.

Petters, M. D., & Kreidenweis, S. M. (2007). A single parameter representation of hygroscopic growth and cloud condensation nucleus activity. *Atmospheric Chemistry and Physics*, *7*(8), 1961-1971, http://doi.org/10.5194/acp-7-1961-2007.

Poschl, U., & Shiraiwa, M. (2015). Multiphase chemistry at the atmosphere-biosphere interface influencing climate and public health in the anthropocene. *Chemical reviews*, *115*(10), 4440-4475, http://doi.org/10.1021/cr500487s.

Pryor, S. C., Joerger, V. M., & Sullivan, R. C. (2016). Empirical estimates of size-resolved precipitation scavenging coefficients for ultrafine particles. *Atmospheric Environment*, *143*, 133-138, http://doi.org/10.1016/j.atmosenv.2016.08.036.

Qi, X. M., et al. (2015). Aerosol size distribution and new particle formation in western Yangtze River Delta of China: two-year measurement at the SORPES station. *Atmospheric Chemistry and Physics Discussions*, *15*(8), 12491-12537, http://doi.org/10.5194/acpd-15-12491-2015.

Ramana, M. V., Ramanathan, V., Kim, D., Roberts, G. C., & Corrigan, C. E. (2007). Albedo, atmospheric solar absorption and heating rate measurements with stacked UAVs. *Quarterly Journal of the Royal Meteorological Society*, *133*(629), 1913-1931, http://doi.org/10.1002/qj.172.

Ramanathan, V., Chung, C., Kim, D., Bettge, T., Buja, L., Kiehl, J. T., Washington, W. M., Fu, Q., Sikka, D. R., & Wild, M. (2005). Atmospheric brown clouds: impacts on South Asian climate and hydrological cycle. *Proceedings of the National Academy of Sciences of the United States of America*, *102*(15), 5326-5333, http://doi.org/10.1073/pnas.0500656102.

Ramanathan, V., et al. (2007). Atmospheric brown clouds: Hemispherical and regional variations in long-range transport, absorption, and radiative forcing. *Journal of Geophysical Research*, *112*(D22), http://doi.org/10.1029/2006jd008124.

Rejano, F., Titos, G., Casquero-Vera, J. A., Lyamani, H., Andrews, E., Sheridan, P., Cazorla, A., Castillo, S., Alados-Arboledas, L., & Olmo, F. J. (2021). Activation properties of aerosol particles as cloud condensation nuclei at urban and high-altitude remote sites in southern Europe. *The Science of the total environment*, *762*, 143100, http://doi.org/10.1016/j.scitotenv.2020.143100.

Rolph, G., Stein, A., & Stunder, B. (2017). Real-time Environmental Applications and Display sYstem: READY [Dataset]. *Environmental Modelling & Software*, http://doi.org/10.1016/j.envsoft.2017.06.025.

Rose, D., Gunthe, S. S., Mikhailov, E., Frank, G. P., Dusek, U., Andreae, M. O., & Poschl, U. (2008). Calibration and measurement uncertainties of a continuous-flow cloud condensation nuclei counter (DMT-CCNC): CCN activation of ammonium sulfate and sodium chloride aerosol particles in theory and experiment. *Atmospheric Chemistry and Physics*, *8*(5), 1153-1179, http://doi.org/10.5194/acp-8-1153-2008.

Rose, D., Nowak, A., Achtert, P., Wiedensohler, A., Hu, M., Shao, M., Zhang, Y., Andreae, M. O., & Pöschl, U. (2010). Cloud condensation nuclei in polluted air and biomass burning smoke near the mega-city Guangzhou, China – Part 1: Size-resolved measurements and implications for the modeling of aerosol particle hygroscopicity and CCN activity. *Atmospheric Chemistry and Physics*, *10*(7), 3365-3383, http://doi.org/10.5194/acp-10-3365-2010.

Saturno, J., et al. (2018). Black and brown carbon over central Amazonia: long-term aerosol measurements at the ATTO site. *Atmospheric Chemistry and Physics*, *18*(17), 12817-12843, http://doi.org/10.5194/acp-18-12817-2018.

Scott, C. E., Arnold, S. R., Monks, S. A., Asmi, A., Paasonen, P., & Spracklen, D. V. (2017). Substantial large-scale feedbacks between natural aerosols and climate. *Nature Geoscience*, *11*(1), 44-48, http://doi.org/10.1038/s41561-017-0020-5.

Sebastian, M., Kanawade, V. P., Soni, V. K., Asmi, E., Westervelt, D. M., Vakkari, V., Hyvärinen, A. P., Pierce, J. R., & Hooda, R. K. (2021). New Particle Formation and Growth to Climate-Relevant Aerosols at a Background Remote Site in the Western Himalaya. *Journal of Geophysical Research: Atmospheres*, *126*(7), http://doi.org/10.1029/2020jd033267.

Seinfeld, J. H., Bretherton, C., & Carslaw, K. S. (2016). Improving our fundamental understanding of the role of aerosol−cloud interactions in the climate system. *Proceedings of the National Academy of Sciences*, *113*(21), 5781-5790, http://doi.org/10.1073/pnas.1514043113/-/DCSupplemental.

Shen, Y., et al. (2019). Estimating cloud condensation nuclei number concentrations using aerosol optical properties: role of particle number size distribution and parameterization. *Atmospheric Chemistry and Physics*, *19*(24), 15483-15502, http://doi.org/10.5194/acp-19-15483-2019.

Singla, V., Mukherjee, S., Safai, P. D., Meena, G. S., Dani, K. K., & Pandithurai, G. (2017). Role of organic aerosols in CCN activation and closure over a rural background site in Western Ghats, India. *Atmospheric Environment*, *158*, 148-159, http://doi.org/10.1016/j.atmosenv.2017.03.037.

Stein, A. F., Draxler, R. R., Rolph, G. D., Stunder, B. J. B., Cohen, M. D., & Ngan, F. (2015). Noaa's Hysplit Atmospheric Transport and Dispersion Modeling System [Dataset]. *Bulletin of the American Meteorological Society*, http://doi.org/10.1175/Bams-D-14-00110.1.

Stevens, R., & Dastoor, A. (2019). A Review of the Representation of Aerosol Mixing State in Atmospheric Models. *Atmosphere*, *10*(4), http://doi.org/10.3390/atmos10040168.

Stolzenburg, M. R., Scheckman, J. H. T., Attoui, M., Han, H.-S., & McMurry, P. H. (2018). Characterization of the TSI model 3086 differential mobility analyzer for classifying aerosols down to 1 nm. *Aerosol Science and Technology*, *52*(7), 748-756, http://doi.org/10.1080/02786826.2018.1456649.

Swietlicki, E., et al. (2017). Hygroscopic properties of submicrometer atmospheric aerosol particles

measured with H-TDMA instruments in various environments—a review. *Tellus B: Chemical and Physical Meteorology*, *60*(3), 432-469, http://doi.org/10.1111/j.1600-0889.2008.00350.x.

Twomey, S. (1959). The nuclei of natural cloud formation part II: the supersaturation in natural clouds and the variation of cloud droplet concentration. *Geofis. Pura Appl.* , *43*, 243–249, http://doi.org/https://doi.org/10.1007/BF01993560.

Ueda, S., Miura, K., Kawata, R., Furutani, H., Uematsu, M., Omori, Y., & Tanimoto, H. (2016). Number–size distribution of aerosol particles and new particle formation events in tropical and subtropical Pacific Oceans. *Atmospheric Environment*, *142*, 324-339, http://doi.org/10.1016/j.atmosenv.2016.07.055.

Varghese, M., Prabha, T. V., Malap, N., Resmi, E. A., Murugavel, P., Safai, P. D., Axisa, D., Pandithurai, G., & Dani, K. (2016). Airborne and ground based CCN spectral characteristics: Inferences from CAIPEEX – 2011. *Atmospheric Environment*, *125*, 324-336, http://doi.org/10.1016/j.atmosenv.2015.06.041.

Vu, D., Gao, S., Berte, T., Kacarab, M., Yao, Q., Vafai, K., & Asa-Awuku, A. (2019). External and internal cloud condensation nuclei (CCN) mixtures: controlled laboratory studies of varying mixing states. *Atmospheric Measurement Techniques*, *12*(8), 4277-4289, http://doi.org/10.5194/amt-12-4277-2019.

Wang, D., Zhou, B., Fu, Q., Zhao, Q., Zhang, Q., Chen, J., Yang, X., Duan, Y., & Li, J. (2016). Intense secondary aerosol formation due to strong atmospheric photochemical reactions in summer: observations at a rural site in eastern Yangtze River Delta of China. *The Science of the total environment*, *571*, 1454-1466, http://doi.org/10.1016/j.scitotenv.2016.06.212.

Wang, H., Zhu, B., Shen, L., An, J., Yin, Y., & Kang, H. (2014). Number size distribution of aerosols at Mt. Huang and Nanjing in the Yangtze River Delta, China: Effects of air masses and characteristics of new particle formation. *Atmospheric Research*, *150*, 42-56, http://doi.org/10.1016/j.atmosres.2014.07.020.

Wang, Q., et al. (2019). Impacts of short-term mitigation measures on PM_{2.5} and radiative effects: a case study at a regional background site near Beijing, China. *Atmospheric Chemistry and Physics*, *19*(3), 1881-1899, http://doi.org/10.5194/acp-19-1881-2019.

Wang, W., et al. (2020). Exploring the drivers of the increased ozone production in Beijing in summertime during 2005–2016. *Atmospheric Chemistry and Physics*, *20*(24), 15617-15633, http://doi.org/10.5194/acp-20-15617-2020.

Wang, Y., et al. (2018a). Characterization of aerosol hygroscopicity, mixing state, and CCN activity at a suburban site in the central North China Plain. *Atmospheric Chemistry and Physics*, *18*(16), 11739-11752, http://doi.org/10.5194/acp-18-11739-2018.

Wang, Y., Vogel, J. M., Lin, Y., Pan, B., Hu, J., Liu, Y., Dong, X., Jiang, J. H., Yung, Y. L., & Zhang, R. (2018b). Aerosol microphysical and radiative effects on continental cloud ensembles. *Advances in Atmospheric Sciences*, *35*(2), 234-247, http://doi.org/10.1007/s00376-017-7091-5.

Weller, R., Schmidt, K., Teinilä, K., & Hillamo, R. (2015). Natural new particle formation at the coastal Antarctic site Neumayer. *Atmospheric Chemistry and Physics*, *15*(19), 11399-11410, http://doi.org/10.5194/acp-15-11399-2015.

Wentworth, G. R., Murphy, J. G., Benedict, K. B., Bangs, E. J., & Collett Jr, J. L. (2016). The role of dew as a night-time reservoir and morning source for atmospheric ammonia. *Atmospheric Chemistry and Physics*, *16*(11), 7435-7449, http://doi.org/10.5194/acp-16-7435-2016.

Wiedensohler, A., et al. (2012). Mobility particle size spectrometers: harmonization of technical standards and data structure to facilitate high quality long-term observations of atmospheric particle number size distributions. *Atmospheric Measurement Techniques*, *5*(3), 657-685,

http://doi.org/10.5194/amt-5-657-2012.

Williamson, C. J., et al. (2021). Large hemispheric difference in nucleation mode aerosol concentrations in the lowermost stratosphere at mid- and high latitudes. *Atmospheric Chemistry and Physics*, *21*(11), 9065-9088, http://doi.org/10.5194/acp-21-9065-2021.

Willis, M. D., et al. (2016). Growth of nucleation mode particles in the summertime Arctic: a case study. *Atmospheric Chemistry and Physics*, *16*(12), 7663-7679, http://doi.org/10.5194/acp-16-7663-2016.

Wu, T., & Boor, B. E. (2021). Urban aerosol size distributions: a global perspective. *Atmospheric Chemistry and Physics*, *21*(11), 8883-8914, http://doi.org/10.5194/acp-21-8883-2021.

Wu, Z. J., et al. (2017). Thermodynamic properties of nanoparticles during new particle formation events in the atmosphere of North China Plain. *Atmospheric Research*, *188*, 55-63, http://doi.org/10.1016/j.atmosres.2017.01.007.

Xu, W., Fossum, K. N., Ovadnevaite, J., Lin, C., Huang, R.-J., O'Dowd, C., & Ceburnis, D. (2021a). The impact of aerosol size-dependent hygroscopicity and mixing state on the cloud condensation nuclei potential over the north-east Atlantic. *Atmospheric Chemistry and Physics*, *21*(11), 8655-8675, http://doi.org/10.5194/acp-21-8655-2021.

Xu, W., Ovadnevaite, J., Fossum, K. N., Lin, C., Huang, R. J., O'Dowd, C., & Ceburnis, D. (2021b). Seasonal Trends of Aerosol Hygroscopicity and Mixing State in Clean Marine and Polluted Continental Air Masses Over the Northeast Atlantic. *Journal of Geophysical Research: Atmospheres*, *126*(11), http://doi.org/10.1029/2020jd033851.

Yang, Z., Xu, L., Tsona, N. T., Li, J., Luo, X., & Du, L. (2021). SO2 and NH3emissions enhance organosulfur compounds and fine particle formation from the photooxidation of a typical aromatic hydrocarbon. *Atmospheric Chemistry and Physics*, *21*(10), 7963-7981, http://doi.org/10.5194/acp-21-7963-2021.

Yu, H., Ren, L., & Kanawade, V. P. (2017). New Particle Formation and Growth Mechanisms in Highly Polluted Environments. *Current Pollution Reports*, *3*(4), 245-253, http://doi.org/10.1007/s40726-017-0067-3.

Yu, Q.-R., Zhang, F., Li, J., & Zhang, J. (2019). Analysis of sea-salt aerosol size distributions in radiative transfer. *Journal of Aerosol Science*, *129*, 71-86, http://doi.org/10.1016/j.jaerosci.2018.11.014.

Yue, D., et al. (2009). Characteristics of aerosol size distributions and new particle formation in the summer in Beijing. *Journal of Geophysical Research*, *114*, http://doi.org/10.1029/2008jd010894.

Zhang, Q., et al. (2017). Variations of aerosol size distribution, chemical composition and optical properties from roadside to ambient environment: A case study in Hong Kong, China. *Atmospheric Environment*, *166*, 234-243, http://doi.org/10.1016/j.atmosenv.2017.07.030.

Zhang, Q., Shen, Z., Lei, Y., Wang, Y., Zeng, Y., Wang, Q., Ning, Z., Cao, J., Wang, L., & Xu, H. (2018). Variations of Particle Size Distribution, Black Carbon, and Brown Carbon during a Severe Winter Pollution Event over Xi'an, China. *Aerosol and Air Quality Research*, *18*(6), 1419-1430, http://doi.org/10.4209/aaqr.2018.01.0007.

Zhang, R., Wang, G., Guo, S., Zamora, M. L., & Wang, Y. (2015). Formation of Urban Fine Particulate Matter. *Chemical reviews*, *115*(10), 3803-3855.

Zhang, Z., Liu, L., Wang, B., Tan, H., Lan, C., Wang, Y., & Chan, P. (2022). Impact of Aerosol Mixing State and Hygroscopicity on the Lidar Ratio. *Remote Sensing*, *14*(7), http://doi.org/10.3390/rs14071554.

Zhao, G., et al. (2021). Impact of aerosol–radiation interaction on new particle formation. *Atmospheric Chemistry and Physics*, *21*(13), 9995-10004, http://doi.org/10.5194/acp-21-9995-2021.